Heliyon 10 (2024) e28253

Contents lists available at ScienceDirect

Heliyon

journal homepage: www.cell.com/heliyon

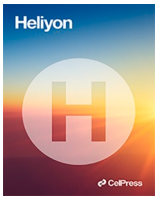

Review article

# Mercury abatement in the environment: Insights from industrial emissions and fates in the environment

Hsin-Chieh Kung [a], Chien-Hsing Wu [b,c], Bo-Wun Huang [d], Guo-Ping Chang-Chien [a,e,f], Justus Kavita Mutuku [a,e,f,*], Wan-Ching Lin [g,h,**]

[a] Institute of Environmental Toxin and Emerging-Contaminant Research, Cheng Shiu University, Kaohsiung, 833301, Taiwan
[b] Division of Nephrology, Department of Internal Medicine, Kaohsiung Chang-Gung Memorial Hospital, Kaohsiung, 83301, Taiwan
[c] Center for General Education, Cheng Shiu University, Kaohsiung 833301, Taiwan
[d] Department of Mechanical and Institute of Mechatronic Engineering, Cheng Shiu University, Kaohsiung City, 833301, Taiwan
[e] Super micro mass research and technology center, Cheng Shiu University, Kaohsiung, 833301, Taiwan
[f] Center for Environmental Toxin and Emerging-Contaminant Research, Cheng Shiu University, Kaohsiung, 833301, Taiwan
[g] Department of Neuroradiology, E-Da Hospital, I-Shou University, Kaohsiung, 84001, Taiwan
[h] Department of Neurosurgery, E-Da Hospital/I-Shou University, Kaohsiung, 84001, Taiwan

ARTICLE INFO

*Keywords:*
Mercury
Emissions
Transformations
Capture & mitigation

ABSTRACT

Mercury's neurotoxic effects have prompted the development of advanced control and remediation methods to meet stringent measures for industries with high-mercury feedstocks. Industries with significant Hg emissions, including artisanal and small-scale gold mining (ASGM)-789.2 Mg $year^{-1}$, coal combustion-564.1 Mg $year^{-1}$, waste combustion-316.1 Mg $year^{-1}$, cement production-224.5 Mg $year^{-1}$, and non-ferrous metals smelting-204.1 Mg $year^{-1}$, use oxidants and adsorbents capture Hg from waste streams. Oxidizing agents such as $O_3$, $Cl_2$, HCl, $CaBr_2$, $CaCl_2$, and $NH_4Cl$ oxidize $Hg^0$ to $Hg^{2+}$ for easier adsorption. To functionalize adsorbents, carbonaceous ones use S, $SO_2$, and $Na_2S$, metal-based adsorbents use dimercaprol, and polymer-based adsorbents are grafted with acrylonitrile and hydroxylamine hydrochloride. Adsorption capacities span 0.2–85.6 mg $g^{-1}$ for carbonaceous, 0.5–14.8 mg $g^{-1}$ for metal-based, and 168.1–1216 mg $g^{-1}$ for polymer-based adsorbents. Assessing Hg contamination in soils and sediments uses bioindicators and stable isotopes. Remediation approaches include heat treatment, chemical stabilization and immobilization, and phytoremediation techniques when contamination exceeds thresholds. Achieving a substantially Hg-free ecosystem remains a formidable challenge, chiefly due to the ASGM industry, policy gaps, and Hg persistence. Nevertheless, improvements in adsorbent technologies hold potential.

## 1. Introduction

Seven decades after documenting its creeping neurotoxicity, mercury exposure is still a concern in the present world. It is among the priority metals significant to public health [1], with key emission sources such as artisanal gold mining, coal combustion, waste

* Corresponding author. Institute of Environmental Toxin and Emerging-Contaminant Research, Cheng Shiu University, Kaohsiung, 833301, Taiwan.
** Corresponding author. Department of Neuroradiology, E-Da Hospital, I-Shou University, Kaohsiung, 84001, Taiwan.
*E-mail addresses:* 6923@gcloud.csu.edu.tw, Justusmuttuku@gmail.com (J.K. Mutuku), 109840@edah.org.tw (W.-C. Lin).

https://doi.org/10.1016/j.heliyon.2024.e28253
Received 29 October 2023; Received in revised form 14 March 2024; Accepted 14 March 2024
Available online 20 March 2024

combustion, cement manufacturing, and metal smelting process [2]. These sources emit elemental mercury ($Hg^0$), which gets oxidized to other forms in the natural environment, including monovalent mercury ($Hg^+$) and divalent mercury ($Hg^{2+}$), and particulate

**Abbreviations**

| | |
|---|---|
| ASGM | Artisanal and small-scale gold mining |
| ATSDR | Agency for toxic substances and disease registry |
| BACT | Best available control technology |
| DMeHg | Dimethylmercury |
| EU | European Union |
| GEM | Gaseous elemental mercury (Hg0) |
| GOM | Gaseous mercury in oxidized |
| Hg | Mercury |
| $Hg^+$ & $Hg^{++}$ | Ionic forms of mercury |
| $Hg^0$ | Elemental mercury |
| HgS | Mercury sulfide |
| LCPUFA | Long-chain polyunsaturated fatty acids |
| MeHg | Methylmercury |
| MC | Minamata convention |
| MOF | Metal-organic framework |
| PHg | Particle-bound mercury |
| PTEs | Potentially toxic elements |
| RGM | Reactive gaseous mercury |
| ROS | Reactive oxygen species |
| SQC | Soil quality criteria |
| TGM | Total gaseous Hg |
| THg | Total mercury |
| TPM | Total particulate mercury |
| TTHQ | Total target hazard quotient |
| UNEP | United Nations Environment Programme |

mercury (PHg). Methylation, a critical conversion, leads to methyl mercury (MeHg) formation, which gets biomagnified up the food chain [3]. Following the Minamata mercury catastrophe in the mid-20th century, the globe implemented stringent measures to limit environmental mercury exposure. Occupational exposure is critical. For instance, the urinary Hg concentrations in dental health medics, chloralkali workers, and the general public are >30 μg $L^{-1}$ [4], 34.3 μg $L^{-1}$ [5], and 1.1 μg $L^{-1}$ [6], respectively.

Within a short-timeframe, Hg induces inflammation, primary paresthesia, nausea, gingivostomatitis, metallic taste, dizziness, and vomiting [7]. In a longer-timeframe, it generates a consistent pattern of irreversible neural dysfunction in the nervous system [8]. Specifically, it causes Alzheimer's disease [9] and multiple sclerosis, leading to cognitive, vision, motor, emotional deficits, and somatosensory [10]. Besides the neurodegenerative disorders, Hg causes cardiomyopathy in the heart, pulmonary fibrosis in the lungs, kidney failure, subsequent renal cancer, and immune disorders [11].

Since Hg, as an element, is indestructible, the Minamata Convention supports the abolition of cinnabar (HgS) mining activities as a crucial strategy for curbing Hg contamination. Hg-free replacements are required to refine silver and gold and manufacture thermometers, fluorescence bulbs, batteries, and other electronic devices [12]. Delayed action will cause growth in legacy emissions, where estimates indicate a 14% decrease in policy impacts on a local scale for every 5-year delay [13]. For inevitable emissions, control measures such as adsorption [14], wet scrubbing [15], oxidation, membrane filtration, precipitation, and electrochemical approaches are adopted to abstract Hg from waste streams. Remediation of contaminated soils, including abandoned gold mines, chloralkaline, and mono vinyl chloride plants, uses physical, chemical, and biological approaches [16].

Previous review articles on Hg have focused on emission sources [17], dispersions [18], adverse effects on humans [19], and emission control and remediation approaches [20]. Due to the evolving nature of new abatement techniques, the latter remains under-explored. This review is based on recent scientific articles gathered using keywords: Hg, emission sources, dispersion, transformations, control, and remediation. It highlights (i) Hg source characterization, dispersion, and regional spatial contributions, (ii) methods of mapping Hg contaminations, and (iii) approaches for capturing Hg emissions and reclamation measures for Hg-contaminated soils. A review of perspectives of the recent techniques applied for Hg control and remediation provides valuable information for protecting human health and the environment, complying with the emission regulations according to the Minamata Convention, and advancing resource recovery and sustainable development goals.

## 2. Primary mercury sources: a comprehensive overview

Several parameters are combined to estimate Hg emissions, including emission factors, statistical data, and consumption of Hg-

containing products [21]. Current annual Hg emissions from natural and anthropogenic sources are approximately 500 Mg and 2449 Mg, respectively, as depicted in Fig. 1. Many uncertainties exist on terrestrial and aquatic Hg re-emission. However, current estimations indicate annual emissions of 1700–5200 Mg [21]. Natural emissions mainly involve gassing off from the soil and earth's crust during normal seepage and volcanic disruptions [22] and from geothermal springs and forest fires [23], as presented in Fig. 1. Traces of Hg in the earth's crust integrate with industrial feedstocks summarized in Table 1, including gypsum, limestone, coal, metal ores, and waste. Eventually, they manifest in artificial activities involving these raw materials, as suggested in Fig. 2a.

According to UNEP, about 45% of the global anthropogenic emissions in 2018 came from Asia, where China notably produced 25.7% [21,24]. East Asia (1053 Mg) is the most dominant source of Hg globally. South America, South Asia, Western Africa, Southeast Asia, and East and Central Africa are other regions with significant Hg emissions, as seen in Fig. 2b. The spatial distribution in anthropogenic Hg emissions is primarily linked to socioeconomic factors [25].

### 2.1. Combustion-related mercury emissions

Global annual Hg emissions from critical combustion sources include artisanal and small-scale gold mining (ASGM), 789.2 Mg [26], coal combustion, 564.1 Mg [27], waste combustion, 316.1 Mg [28], cement manufacturing, 224.5 Mg [29], and smelting of non-ferrous metal ores, 204.1 Mg [24] as presented in Fig. 2a. Altogether these combustion sources contribute about 85.7% of the Hg emitted globally and significantly affect Hg ambient air background concentrations.

In ASGM, an amalgam of gold containing silt and Hg extract is heated, releasing Hg vapor into the ambient air [30]. This method is applied to process 20–30% (500–800 tons) of the gold produced globally. In 2018, the United Nations Environmental Programme (UNEP) reported that ASGM made about 37.7% (837 tons) of the total Hg emissions [31,32]. Weighted linear projections into 2022 indicate that it produced 789 Mg. According to the Global Mercury Assessment 2018 (2018 GMA), Indonesia and the Philippines in Southeast Asia, China in East Asia and Peru, Columbia, Bolivia, Brazil, Venezuela, and Ecuador in Southern America, and Sudan in Africa are the countries with the most mercury-intensive ASGM sectors [33]. Despite being active signatories in the Minamata Convention (MC), these countries are likely to continue unabated ASGM processes due to high gold prices and the proliferation of Hg amalgamation [34].

According to the International Energy Agency, coal is currently the most critical energy source globally, with a consumption of 8 billion tons in 2022 [35]. Coal contains different forms of Hg, including HgS, MeHg, and clay-bound Hg [36]. The concentrations vary with the type of coal, whereby lignite yields more Hg than bituminous and sub-bituminous [37]. Typical contents for coal from China, USA, SA, Poland, and Australia are summarized in Table 1, where they range from 50 to 200 μg $kg^{-1}$, with a global average of 100 μg $kg^{-1}$. Homogeneous and heterogeneous reactions involving the above mentioned compounds release Hg during coal combustion. Globally, 560 Mg of Hg is released this way each year, as seen in Fig. 2a, making coal combustion the second largest source. This Hg emission source will likely remain constant in the short term due to coal's central role in energy production for big economies such as China, India, and the USA [36]. China is responsible for about 50% of the annual global coal consumption, followed by India (11%), the USA (8.9%), Japan (3.2%), and Russia (2.5%). Other than the USA, all the top five coal consumer countries are in Asia, and this is reflected in the distributions of emissions presented in Fig. 2b.

Among the different types of wastes converted to energy in incinerators, municipal solid waste (MSW), whose global consumption in 2022 was about 1.34 billion tons, has the highest Hg content ranging between 32.8 and 46222 μg $kg^{-1}$, as seen in Table 1 [38]. Consequently, waste combustion ranks third worldwide in Hg sources, as seen in Fig. 2a, contributing about 13% of global Hg

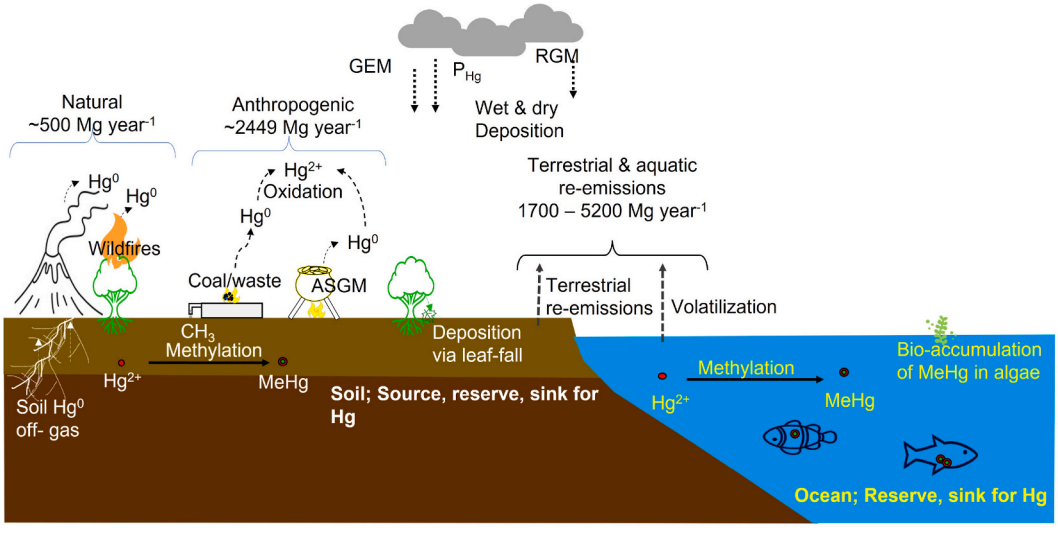


**Fig. 1.** Schematic representation of the proportions of mercury emitted from natural and anthropogenic sources, dispersion, and their fates in the environment, adapted from [21,193].

**Table 1**
The concentrations of Hg in different commonly used raw materials for industrial purposes.

| Raw material | | Hg composition (μg $kg^{-1}$) | Common application | Reference |
|---|---|---|---|---|
| Limestone | | 16.2–33.4 | Cement production | [29] |
| Gypsum | | 220–20600 | Cement production | [120] |
| | | 160–1482 | FGD in CPPs | [154] |
| Coal | China, SA | 200 | Power generation/steel industry | [36] |
| | USA | 170 | | |
| | Indonesia | 100 | | |
| | Poland | 50 | | |
| | Australia | 60 | | |
| RDFs | | 0.1–2.2 | Power generation | [155] |
| Sewage Sludge | | 3.5–7.7 | Power generation | |
| MSW | | 32.8–46222 | Landfill | [156] |
| Rubber waste | | 60.2–96.9 | Power generation | [29] |

**Note:** FDG represents flue gas desulfurization.
RDFs represent refuse-derived fuels.
SA represents South Africa.
MSW represents Municipal solid waste.
CFPP represents coal fired power plants.

emissions [39]. This is mainly fueled by rapid urbanization and the generation of large volumes of waste. Gypsum, a raw material in cement manufacturing, is among the raw materials with the highest concentrations of Hg. Its global consumption in 2022 was about 150 million tons [38]. As seen in Table 1, limestone is also critical for cement manufacturing, with Hg concentrations of about 16.2–33.4 μg $kg^{-1}$. Consequently, cement production ranks fourth in global Hg emissions, as presented in Fig. 2a, contributing about 9% [39]. Inadequate Hg abstraction while processing non-ferrous metals, including zinc and lead in rotary kilns and copper in sintering furnaces, contribute about 8% of global Hg emissions, ranking fifth globally, as seen in Fig. 2a [40].

### 2.2. Mercury contamination in aquatic ecosystems

Industrial processes releasing Hg into wastewater include chloralkali plants, vinyl chloride monomer plants, coal slime water, oil refinery processes, dental amalgam, chemical plants, and leakage from contaminated soils [41]. Wastewater treatment plants and desulfurization wastewater from coal-fired power plants [15] on the coast release their wastewater into the sea. Hg emissions from mining activities, such as gold extraction, contaminate nearby soils and waters through infiltration. In an investigation of river fishes in Peru, the Hg content in fish near mining activities exceeded that of fish far from the mining activities [42]. The soil in an active mining site in Ghana had Hg concentrations of 71 mg $kg^{-1}$ [30]. The grounds in the surroundings of chloralkali plants have Hg contents as high as 1150 mg $kg^{-1}$ [21].

Estimations show dental clinics primarily contribute about 36% of Hg in municipal wastewater [43]. Dental amalgam comprises 50% liquid Hg mixed with powdered silver, tin, and copper [44]. During filling, dental professionals are exposed to Hg fumes. Besides dental amalgams, Hg is a joint active agent in disinfectants, diagnostic agents, and diuretics, commonly applied in hospitals [45]. Consequently, hospitals significantly contribute to Hg concentrations in wastewater, whereby the concentrations vary with the treatment technology adopted, such as express release into the ecosystem, co-treatment, and special treatment.

Chloralkaline plants equipped with Hg electrodes [46] and vinyl chloride monomer plants with Hg catalysts [2] are still operational in some countries. Hg leakages from these industries contaminate the marine environments. Another significant source of Hg is wastewater released from organic chemical plants. For instance, pharmaceutical wastewater affects Hg pollution due to methyl groups such as tetracyclines (TC) and oxytetracyclines (OC), which enhance MeHg formation, as well as other residues such as carbon nanotubes, which prevent methylation [14]. The release of high-nutrient water leads to eutrophication, which provides the required organic matter in sediments. Furthermore, decomposition creates anoxic environments favorable for methylation, and the organic matter from the algae bloom bioaccumulates MeHg [47].

## 3. Mercury dispersion and environmental impact

For an enhanced understanding of Hg's dispersion and fate, it is imperative to explore the diverse forms of Hg in the environment [48]. Classification is based on three fundamental approaches: oxidation states, physical forms, and chemical properties. Based on the oxidation states, there are three forms of Hg: gaseous elemental mercury (GEM), $Hg^{+}$, and $Hg^{2+}$ [23]. GEM is stable and is common in ambient air and heavily polluted soils. About 60% of global Hg is emitted in this form [24]. $Hg^{+}$ is highly unstable and rarely found in any environmental matrix [49]. On the other hand, $Hg^{2+}$ is stable and commonly deposited through dry deposition, making it the most dominant in soil [21]. The second approach, regarding chemical form, classifies Hg into organic and inorganic forms. The organic forms include methylmercury (MeHg), ethylmercury (etHg), and dimethylmercury (diMeHg), while the inorganic ones include $HgCl_2$, HgS, and HgO. MeHg, the most toxic form of Hg, makes up 95% of the Hg in aquatic life [50]. The third approach classifies Hg based on its volatility [20] and solubility in water [21]. To determine Hg concentrations in different environmental compartments, computational models use source contributions, distance factors, and Hg transformation data [36].

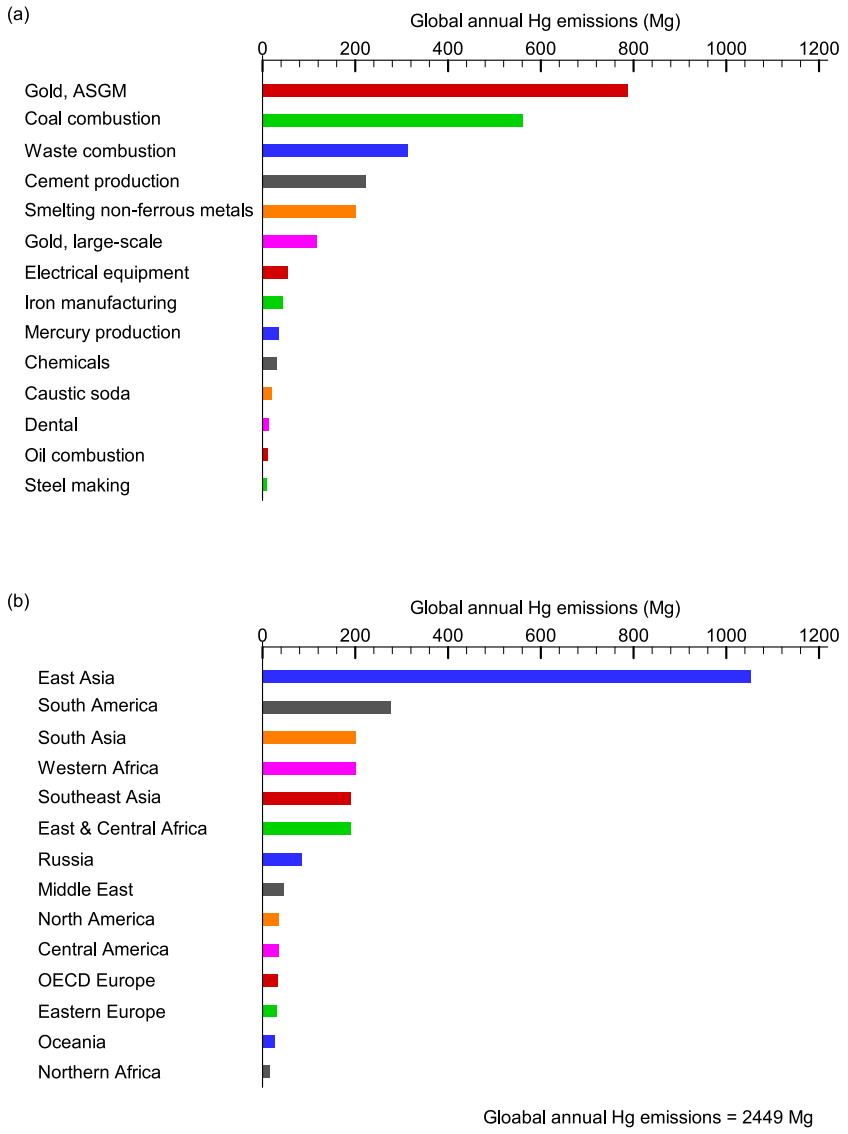


**Fig. 2.** Weighted linear estimations of global anthropogenic Hg emissions in 2022 by (a) industry and (b) region, modified from a previous investigation [32].

### *3.1. Mercury in the atmosphere: transformation mechanisms and consequences*

Overall, Hg ambient air background concentrations for remote and urban/sub-urban areas are 1–10 ng $m^{-3}$ and 1–20 ng $m^{-3}$, respectively [51]. However, the ambient air concentrations in the vicinities of localized sources can reach 10500–46300 ng $m^{-3}$ during volcanic activities, for instance, on Nisyros Island, Greece [52]. The general ranking for the concentrations is presented in Table 2, where remote locations < urban areas < Hg related industries < Hg mines. In the atmosphere, Hg exists as GEM, gaseous oxidized/reactive gaseous mercury (RGM), PHg, and methylmercury (MeHg) [37]. GEM makes 95% of the total Hg in the atmosphere, is highly insoluble in water, has long lifespans, and undergoes long-range transportation, contributing to the global pool of Hg [21]. In an investigation in the Strait of Taiwan, total gaseous mercury (TGM) and PHg had partitions of 96%–97% and 3%–4%, respectively. GEM, RGM, and PHg had concentrations of 1.73 ng $m^{-3}$, 12.1 pg $m^{-3}$, and 2.3 pg $m^{-3}$, respectively [53]. At a temperature of 25 °C, RGM has a water solubility of $1.4 \times 10^{6}$ M $atm^{-1}$, while that of elemental carbon is $1.1 \times 10^{-1}$ M $atm^{-1}$ [54]. PHg forms when GEM and RGM condense on PM. It is mainly deposited near emission sources, impacting the local concentrations in soil, sediment, and aquatic systems [55]. Collectively, PHg and RGM form 5% of the ambient air Hg contents, last for days to weeks in the atmosphere, and deposit easily through wet and dry deposition [56]. Essential Hg combustion sources also produce SOx and NOx, affecting Hg's atmospheric chemistry and environmental fate [39]. Specifically, they oxidize $Hg^{0}$ to $Hg^{2+}$, thereby increasing the proportion of RGM and improving the likelihood of wet deposition.

**Table 2**
Concentrations of Mercury in different environmental matrices.

| Environmental matrix | Details | Location | Type of Hg | Concentration | Reference |
|---|---|---|---|---|---|
| **Hg in Air** | Hg mine | Wanshan, Guizhou, china | TGM | 17.8–102 | [157] |
| **Concentrations (ng $m^{-3}$)** | | Wuchuan, Guizhou, china | | 19.5–2110 | [158] |
| | | Lanmuchang, Guizhou, china | | 7.9–468 | [159] |
| | 70 m from a chloralkali plant | Bohus, Sweden | TGM | 55 | [160] |
| | 560 m from a chloralkali plant | | | 3.5 | |
| | Urban | Taipei, Taiwan | TGM | 6.9–120 | [161] |
| | Urban | Hsinchu, Taiwan | TGM | 7.8 | |
| | Urban | Tokyo, Japan | TGM | 2.9 | [23] |
| | Urban | Tainan, Taiwan | PGH | 8.4 | [23] |
| | Urban | Seoul, Korea | PGH | 0.03 | |
| **Hg in Soil** | Topsoil (0–20 cm) | Beijing, China | THg | 0.02–9.4 | [162] |
| **Concentrations (μg $g^{-1}$)** | Topsoil (5–10 cm) | Forest | TGM | 0.0009 ± 0.0008 | [65] |
| | | Grass field | TGM | 0.0006 ± 0.0007 | |
| | – | Reno, Nevada, USA | THg | 0.01–27.7 | [163] |
| | Soil with no bird droppings | Tongli Wetland, Wijiang city, East China | THg | 0.2 ± 0.03 | [164] |
| | Soil with bird droppings | | THg | 0.1 ± 0.04 | |
| | Wetland soil | Dongting Lake, China | THg | 0–1.7 | [165] |
| | Acetic acid plant | Guizhou, China | THg | 1.1–3.7 | [166] |
| **Hg in Water** | Surface water | Asia | THg | 0.1–10 | [99] |
| **Concentrations (ng $L^{-1}$)** | Groundwater | Asia | THg | 0.05–5 | |
| | Non-ferrous metal mine | Zijiang River and South Dongting Lake, Hunan Province, China | THg | 38.1 ± 27.1 | [73] |
| | | | PHg | 25.2 ± 26.8 | |
| | | | DHg | 12.9 ± 9.6 | |
| | | | DMeHg | 0.3 ± 0.1 | |
| | Muddy inter-tidal zones | Qeshm, Persian Gulf, Iran | DHg | 350 ± 20 | [167] |
| **Hg in Sediment** | Influenced by industrial emissions | SJ mangrove, Shenzhen, China | THg | 500–620 | [168] |
| **Concentrations (ng $g^{-1}$)** | Influenced by emissions from Guayaquil city | Salado Estuary, Ecuador | THg | 1200–2760 | [169] |
| | Influenced by untreated domestic and industrial wastes | Guanabara Bay, Brazil | THg | 520–2380 | [170] |
| | 35 lakes | China | THg | 234.2 ± 152.9 | [73] |
| | | | DMeHg | 0.5 ± 0.2 | |
| **Hg in Biota** | 117 Yellowfin tuna samples | Different locations | MeHg | 0.03–0.8 | [171] |
| **Concentrations (mg $kg^{-1}$)** | 176 Swordfish samples | Sri Lanka | THg | 0.2–2.6 | [88] |
| | Golden threadfin bream | South China sea | MeHg | 23.5–253 | [86] |
| | | | THg | 27.9–455 | |
| | Thornfish | South China sea | MeHg | 36.8–358 | |
| | | | THg | 55.3–1172 | |
| | Aquaculture fish, (Tilapia, Grass carp, Big head carp) | Guangdong province, South China | THg | 7.8–64.2 | [172] |
| | Mariculture fish (Red drum, snubnose & crimson snapper) | | THg | 59.2–71.7 | |
| | Ocean Fishery, (Hairtail, gold thread, & Common mullet) | | THg | 7–71.8 | |

Note; THg represents total mercury.
MeHg represents methylmercury.
DMeHg represents dissolved methylmercury.
PHg represents particulate mercury.
DHg represents dissolved total mercury.

Regions around the equator experienced the highest wet deposition rates under windy and low atmospheric pressures, which expedite condensation and deposition. Those far from the equator, characterized by cold snow precipitation, experience low wet deposition rates, while the highest dry deposition rates are experienced during anticyclones and in high-altitude areas [57]. The range for the deposition flux of atmospheric Hg in urban areas in China was 43.06–500.6 μg $m^{-2}$ $year^{-1}$ [23], while that of remote areas was 10–50 μg $m^{-2}$ $year^{-1}$ [37]. In an investigation by Ref. [58], in rural and urban areas in Changchun city, China, dry deposition fluxes were 98 μg $m^{-2}$ $year^{-1}$ and 166 μg $m^{-2}$ $year^{-1}$ while wet deposition fluxes were 64 μg $m^{-2}$ $year^{-1}$ and 152 μg $m^{-2}$ $year^{-1}$.

### *3.2. Soil and water: the hidden reservoirs of mercury*

Soil is Hg's source, reservoir, and sink [59]. The global Hg concentration in topsoil is approximately 1.1 million tons. Between 60 and 90% of terrestrial Hg deposition occurs via leaf fall [60], while dry and wet deposition [61] account for the rest. The uptake of dissolved $Hg^{2+}$ through the roots is plants' dominant method of Hg accumulation. A small portion is also up-taken through stomatal

exposure. Plants recycle Hg through leaf fall [60,62]. This affirms the role of vegetation in Hg dispersion and transformation in the environment, as seen in Table 3, where open sites had higher wet and dry deposition than subtropical forests [63]. Ornithogenic sediments from seabird droppings also significantly affect Hg concentrations in the soils near their habitats [2].

In the soil, Hg partitions more to finer particles <63 μm than coarse soil particles. Other factors determining the fate of $Hg^{2+}$ deposited on the topsoil include soil's redox potential, biological and chemical soil properties. About 45–70% of initially deposited $Hg^{2+}$ is reduced to $Hg^0$ and re-emitted to the atmosphere [52]. The rest is sequestered in terrestrial and aquatic habitats. The multidirectional exchange of Hg involving deposition, volatilization, and leaching processes is critical to the biogeochemical Hg cycle [21].

Hg volatilization from the soil and water surfaces is affected by the concentrations of Hg and organic compounds in the soil, air oxidation potential, and weather conditions, including solar radiation, temperature, humidity, and wind [64]. The soil's total gaseous mercury (TGM) is higher in summer and spring compared to the cold winter and fall [65]. Typical volatilization rates are presented in Table 3, where undisturbed non-geologically and thermally enriched locations have volatilization rates lower than 1 ng $m^{-2}$ $h^{-1}$, while contaminated sites and vicinities of base metal smelters had rates exceeding 5000 ng $m^{-2}$ $h^{-1}$ [21]. Furthermore, non-vegetated areas had higher volatilizations than vegetated ones.

Hg from heavily polluted soils infiltrates groundwater, ocean, and other aquatic environments. In marine environments, sediments are the most important sink for Hg [66]. In a global survey on Hg concentrations in marine sediments conducted in 2014, the Persian Gulf and Minamata Bay had the highest Hg concentrations at 3.2 mg $kg^{-1}$ and 2.3 mg $kg^{-1}$ of dry weight, respectively [67]. Among the concentrations in aquatic environments, the dissolved Hg (DHg) in Qeshm, Persian Gulf, Iran, is significantly higher, as presented in Table 2, implying that the marine species from this area have higher Hg contents. In the Rhine River, Switzerland, 91% of the Hg pollution was derived from wet and dry deposition, while the rest originated from wastewater [68].

Hg methylation, an essential process for incorporating MeHg neurotoxin into the food chain [69], is reversible, where both the forward and backward reactions depend on light and bacteria. Currently, no techniques differentiate formation from abiotic and biotic mechanisms. However, abiotic formation mechanisms are insignificant, and therefore, the latter dominates methylation in marine environments facilitated by ionic Hg and organic matter [70]. In anoxic environments in the seawater column, anaerobes with HgcAB gene cluster and sulfate-reducing bacteria (SRB) perform methylation [71]. In oxic environments, methylation occurs through methyl donation from organic compounds or organometallic complexes [70]. Methylation rates are high in mangrove sediments, lacustrine environments, and estuaries since they contain high concentrations of organic matter, high sulfate, and SRB, as evident in an estuarine environment, whereby the average MeHg concentration was 880 ng $g^{-1}$ [72]. The high efficiency of SRB is due to acidic and anaerobic conditions [73]. High pH lowers the methylation via SRB by decreasing Hg and $SO_4^{2-}$ content [71].

Demethylation in marine and lacustrine environments is facilitated by light or microorganisms. The former is the dominant demethylation mechanism, whereby $Hg^0$ detaches from the methyl group under UV radiation in surface waters and sediments [74]. An additional 700 Mg of $Hg^{2+}$ is emitted each year during the decomposition of organic matter [75]. This process converts MeHg to less toxic $Hg^0$ and $Hg^{2+}$, posing risks and contributing to the overall Hg cycle.

**Table 3**
Fluxes between ambient air and the soil.

| Transfer process | Location | Flux (ng $m^{-2}$ $h^{-1}$) | Details of study location | Reference |
|---|---|---|---|---|
| Volatilization | – | <1 | Undisturbed & thermally enriched | [21] |
| | – | >5000 | Contaminated | [21] |
| | Tuscaloosa, Alabama (USA) | 4.5 | Undisturbed Residential | [173] |
| | | 1.4 | Undisturbed Industrial | |
| | | 2.1 | Undisturbed Commercial | |
| | | 0.9 | Undisturbed Mixed land use | |
| | China | 14.2 | Subtropical forests | [63] |
| | | 20.7 | Open sites | |
| | North America | 0.9 ± 0.7 | Grassland | [174] |
| | North China plain | 5.5 ± 21.7 | Corn-wheat rotation cropland | [175] |
| | New York | 0.7 ± 1.8 | Intact forest | [176] |
| | | 9.1 ± 2.1 | Post deforestation | |
| | Brazil | 0.3 ± 0.1 | Intact forest | |
| | | 21.1 ± 0.4 | Post deforestation | |
| | | 74.9 ± 0.7 | Post burning | |
| Deposition | Canada, Manitoba | 3.8 | Closed base metal smelter | [55] |
| | | >5000 | Operating base metal smelter | |
| | Taichung, Taiwan | 52.9 ± 18.7 | Suburban and industrial site | [28] |
| | Guizhou, China | 38.9–270.8 | Urban | [177] |
| | Changchun, China | 4.9 | Urban | [23] |
| | Shenandoah National | 4.8 | Spring | [178] |
| | Park, Virginia (USA) | 2.5 | Summer | |
| | | 0.3 | Fall | |
| | | 4.1 | Winter | |
| | North America | 0.7 | Grassland sites | [174] |
| | Asia | 1.2 | Grassland sites | |
| | Bolivian Andes | 6.3 | Andean silver ores | [179] |

### 3.3. Bioaccumulation and risks: mercury's impact on the ecosystem and human health

The Hg in contaminated soil and water environments bioaccumulate and undergo biomagnification in organisms within those habitats. In plants, translocation affects Hg concentration in the above-ground shoots for plants such as rice, a semi-aquatic plant that bioaccumulates Hg from groundwater [76]. MeHg is the predominant form of Hg in fish, making about 70–95% of the total Hg composition, depending on the trophic level [77].

Aquatic species experience direct exposure to MeHg by ingesting seawater and food and indirectly through absorption via permeable membranes, where susceptibility is mechanistically linked to habitat range, trophic level, and weight of organisms [78]. To safeguard humans against contaminated seafood, the regulatory limits for THg and MeHg in aquatic species are 0.5–1 mg $kg^{-1}$ and 0.1–0.3 mg $kg^{-1}$, respectively [79]. Specific regulatory limits by health regulatory agencies are USFDA- 1 mg $kg^{-1}$ [80], EU-0.5 mg $kg^{-1}$ [81], Food Standard Australia NewZealand-1 mg $kg^{-1}$ [82], and Canadian food inspection agency-0.5 mg $kg^{-1}$ [83]. Due to a lack of seafood quality controls, low-income countries usually consume fish with high Hg concentrations [30,84]. Aquatic species from highly polluted marine habitats, for instance, the South China Sea, exceed the safe seafood quality controls as seen in Table 2.

Since Hg levels are proportional to depth in the ocean water column, the general ranking of Hg levels in aquatic species is benthos > mesopelagic > epipelagic organisms [85]. Seemingly, carnivorous fish such as *Pinirampus pirinampu* have higher concentrations of Hg compared to omnivorous ones such as *Hypophthalmus marginatus* and herbivorous ones such as *Leporinus affinis* [86,87]. Furthermore, larger fish, in terms of length and weight, have higher MeHg content [88]. Tuna, which sits near the top of the food chain, contains more MeHg than salmon in the middle of the food chain [89]. In an investigation by Ref. [90], swordfish and sharks had Hg concentrations of $0.77 \pm 0.83$ mg $kg^{-1}$ and $0.73 \pm 0.54$ mg $kg^{-1}$, respectively, exceeding the safe human limits for seafood in the EU and Canada.

In humans, Hg causes neurological disorders. For instance, after ingesting Hg-contaminated bread in Iraq, people experienced primary paresthesia [91]. Hg at the CNS disturbs the blood-brain barrier, facilitating the penetration of toxins inside the brain [92]. Elemental Hg and MeHg are highly lipophilic, bypassing the placenta, accumulating in the fetus's tissues, and influencing neurodevelopment in children [93]. Consequently, their neurotoxic effects on the unborn and children exceed that of adults [94]. Specifically, it damages developing brains, reduces IQ, and increases the risk of autism, ADHD, and learning disorders in children [11]. In Wanshan, China, children with hair Hg concentrations of 1 μg $g^{-1}$ or higher were 1.58 times more likely to have an IQ score below 80 [95]. In addition to neurological disorders, Hg also causes cardiomyopathy in the heart [96], pulmonary fibrosis in the lungs [97], kidney failure, and subsequent renal cancer [98]. Due to the above mentioned adverse effects, it is prudent to curb Hg emissions from significant emissions.

## 4. Strategies for mercury control and environmental remediation

The "14th International Conference on Mercury as a Global Pollutant (ICMGP) in Krakow, Poland 2019″ held a session on managing Hg-containing wastes such as flue gas and wastewater, whose inadequate containment leads to environmental leaching and soil contamination [99]. In the session, the indestructible nature of Hg was reiterated, and measures stipulated the Minamata Convention [100] for abstracting Hg emissions, including source- [101], in-bed-, end-of-pipe-capture, and safe storage [102].

In practice, Hg in flue gas is captured through the multi-component arrangement of conventional air pollution control devices (APCDs) composed of selective catalytic reactors (SCR), fabric filters (FF) or electrostatic precipitators (ESP), and flue gas desulfurizer (FGD), with removal rates ranging from 68 to 91% [103]. The Hg capture efficiencies reported here are incidental since the SCR and FGD are primarily applied for nitrogen oxide ($NO_x$) control [104] and sulfur dioxide ($SO_2$) removal [105]. The mechanism of Hg extraction for the respective devices involves the oxidation of $Hg^0$ by SCR, the capture of PHg by FF and ESP, and $Hg^{2+}$ removal by FGD [36]. Municipal waste incinerators fitted with fixed bed absorbers, wet scrubbers, and fabric filters with carbon injection had Hg removal efficiencies of 75–82% [106].

Currently, available approaches for removing Hg from wastewater include chemical precipitation [107], reverse osmosis, membrane separation [108], electrolytic processes [109], photo remediation, floatation, solvent extraction, photocatalytic approaches, and adsorption [110,111]. Another strategy involves the oxidation ditch process, where microorganisms consume MeHg before filtration in the final sludge [112]. The injection of eutrophic waters with $O_2$ nanobubbles slows methylation by inhibiting the growth of anaerobic methylating bacteria [113]. These conventional wastewater treatment processes remove 70% of MeHg and 90% of total Hg from influent municipal wastewater [114].

Besides adsorption, the other methods have significant drawbacks, including inapplicability for low Hg concentrations, energy and cost-intensive, need for pretreatments, and excessive sensitivity to environmental parameters such as temperature, pH, and presence of solvents [115]. Therefore, this section emphasizes adsorption due to its versatility compared to other methods.

### 4.1. Recent techniques for adsorbing mercury from flue gas

Source control for Hg is only accomplished through coal washing, where the Hg removal efficiencies for traditional and modern coal washing are about 38.8% and 65–90%, respectively [36]. Traditional coal washing is based on density separation and hence its low Hg removal efficiency [116]. Modern coal washing applies chemical binders such as polymers, surfactants, and sorbents, and froth floating hence its high removal efficiencies [117]. Residual Hg after coal washing usually ends up in the combustion flue gas streams, where they are eliminated via in-bed- and end-of-pipe-capture techniques.

Two key strategies for capturing mercury (Hg) in flue gas streams involve: meticulously controlling the combustion process and

integrating adsorbents with filtration mechanisms [118]. The first approach controls the combustion process to retain portions of unburnt carbon in the flue gas stream. This is crucial for GEM adsorption and further oxidation of $Hg^0$ for easier removal [119]. An extension of this first approach involves the application of fly-ash-based adsorbents, whereby 1% of the fly ash (containing unburnt carbon) is abstracted from the filtration chambers, activated, and recycled back to the flue gas, as indicated in Fig. 3a. This approach is suitable because fly ash contains active promoters of $Hg^0$ oxidation such as $Al_2O_3$, $SiO_2$, $Fe_2O_3$, CuO, and CaO [120]. Furthermore, the irreversibility of this process prevents leaching once fly ash is disposed of in landfills or ash ponds [121]. The second approach involves actively injecting adsorbents, shown in Fig. 3a, which play the same role as unburnt carbon. The adsorption potential is determined by demarcation, catalytic oxidation, and synergism with Hg. Demarcation characterizes the surface using scanning electron microscopy (SEM), atomic force microscopy (AFM), and spectroscopic techniques, and Brunauer-Emmet-Teller (BET) [107]. Catalytic oxidation assessment scrutinizes the synergistic interplay among oxidizing agents, orchestrating the transformation of $Hg^0$ into oxidized mercury species. This transformation enhances subsequent removal by the adsorbent, contributing to a more productive mercury capture process [122].

As summarized in Table 4, the main categories for fixed bed absorbents include carbonaceous, metal-, and polymer-based adsorbents [118]. Due to the inert nature of $Hg^0$, abstracting it using adsorbents presents a significant challenge. Therefore, to improve the adsorption efficiencies, oxidizing agents such as $O_3$, $Cl_2$, HCl, $CaBr_2$, $CaCl_2$, and $NH_4Cl$ are injected into the flue gas stream to oxidize $Hg^0$ to $Hg^{2+}$ for easier adsorption. Recently developed oxidants such as graphene composites (Mn–Ce-RGO), $RuO_2|CeO_6Zr_{0.4})_2$, vanadium silica, and Fe–Ce mixed oxides are combined with conventional adsorbents for higher adsorption efficiencies [107]. The presence of functional groups also affects the adsorption potential. Surface functional groups with high affinity for Hg, including thiols (-SH), sulfonate ($SO_3H$), carboxy (-COOH), amine ($-NH_2$), hydroxyl (-OH), and phosphonate ($-PO_3H_2$) [123] are grafted onto conventional adsorbents to improve the adsorption efficiencies. The performance of an adsorbent is also affected by the leachability of Hg after adsorption. Leachability is affected by the strength of the attraction between the adsorbate and the adsorbent represented by the equation in Table 5, by which adsorption is classified into physical, chemical, and ion exchange, for $E < 8$ kJ/mol, 8 kJ/mol $< E <$ 16 kJ/mol, $E >$ 16 kJ/mol, respectively [111].

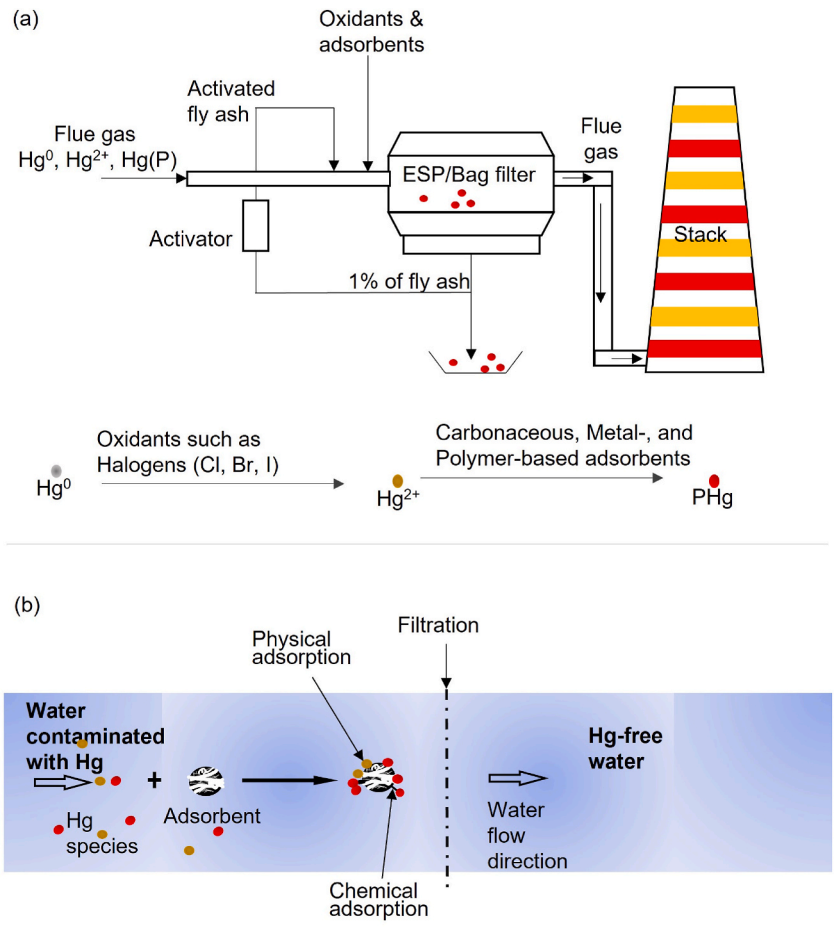


**Fig. 3.** Typical set-up for abstracting Hg from (a) flue gas, adapted from Ref. [118] and (b) wastewater using sorbents, adapted from Ref. [194].

**Table 4**
The adsorption potentials of different mercury adsorbents.

| Sorbent | | Hg Species | Operation condition | BET SA ($m^2 \cdot g^{-1}$) | Pore volume ($cm^3\ g^{-1}$) | Binding Energy (kJ $mol^{-1}$) | Qmax ($mg \cdot g^{-1}$) | Reference |
|---|---|---|---|---|---|---|---|---|
| Carbonaceous | $AC_B$ | | | | | | 0.2 | [121] |
| | AC from bituminous coal infused with 10% S | | | | | | 3 | |
| | AC from bituminous coal infused with 30% $SO_2$ | | | | | | 0.5 | |
| | AC from fluid coke infused with 30% $SO_2$ | | | | | | 0.5 | |
| | AC from mango seed infused with $Na_2S$ | $Hg^{2+}$ | pH of 5 | 2–33 | | | 85.6 | [180] |
| | Brazilian Pepper Biochar Pyrolysed at 300 °C | | 22 ± 0.5 °C, pH of 2–8 | | | | 24.2 | [124] |
| | Brazilian Pepper Biochar Pyrolysed at 450 °C | | | | | | 18.8 | |
| | Brazilian Pepper Biochar Pyrolysed at 600 °C | | | | | | 15.1 | |
| Metal-based | Vermiculite | $Hg_{aq}$ | 30 °C, pH of 4–5 | 4.1 | 0.007 | −37.9 | 0.5 | [181] |
| | Montmorillonite | $Hg_{aq}$ | | 71.5 | 0.122 | −9.3 | 0.8 | |
| | Dimercaprol grafted on vermiculite | $Hg_{aq}$ | | 0.9 | 0.004 | −65.6 | 5.0 | |
| | Dimercaprol grafted on montmorillonite | $Hg_{aq}$ | | 54.2 | 0.1 | 8.8 | 3.2 | |
| | $Fe_6Mn_{0.8}Ce_{0.2}O_y$ | | | 106.1 | | | | [182] |
| | Fe-containing sewage sludge activated with $H_2SO_4$ | | | | | | 14.8 | [183] |
| | β- Zeolites | $Hg_{aq}$ | | 575 | | | 1.9 | [128] |
| | Zeolite Y | $Hg_{aq}$ | | 660 | | | 1.6 | |
| | Modernite | $Hg_{aq}$ | | 250 | | | 0.8 | |
| | Calcium bentonite | | 25 °C | | | | 1.9 | [184] |
| | CaO on mesoporous silica | $Hg^{2+}$ | | 33.9 ± 10.8 | 0.13 ± 0.04 | 21.5 | | [126, 185] |
| | $CaCO_3$ on mesoporous silica | $Hg^{2+}$ | | 8.0 ± 1.8 | 0.05 ± 0.02 | | | [126] |
| | 2% Mn/ITQ-2 | $Hg^0_{aq}$, | | 90.7 | 0.65 | | 1.9 | [186] |
| | 5% Mn/ITQ-2 | $Hg^{2+}_{aq}$ | | 92 | 0.68 | | 2.0 | [123] |
| | 2% Co–2% Mn/ITQ-2 | | | 90 | 0.62 | | – | [183] |
| | 2% Co–5% Mn/ITQ-2 | | | 91.8 | 0.67 | | 3.5 | [128] |
| | Mordenite | $Hg_{aq}$ | | 250 | | | 0.8 | |
| Polymer-based | Polyacrylonitrile bound to polystyrene and cyano moiety with hydroxylamine | | | | | | 526.9 | [187] |
| | Amidoxime acrylonitrile/methyl acrylate | | | | | | 521.5 | [188] |
| | Amidoximated wheat straw | | | | | | 942.7 | [111] |
| | Polypropylene grafted with acrylonitrile + diethylene triamine | | | | | | 657.9 | |
| | Polyacrylonitrile-2-amino-1,3,4-thiadiazole | | pH, 6.5 | | | | 456.1 | |
| | Poly(Zirconyl methacrylate-*co*-1-vinyl imidazole) | | pH 7 ± 0.2 | 402 | 0.40 | 8–16 | 168.1 | [123] |
| | Polymerized benzene-1,3,5-triyltris (9H-carbazol-9-yl) methanone | $Hg^{2+}{}_{(g)}$ | 273 K | 613 | 0.57 | – | 335 | [189] |
| | Polymerized 3,5-divinylbenzyl chloride with azobisisobutyronitrile | $Hg^0$, $Hg^{2+}{}_{(g)}$ | | | | | 1216 | [190] |
| | | $Hg^0$, $Hg^{2+}{}_{(aq)}$ | pH, 3-10 | 1061 | – | – | 630 | |
| | Magnetic mesoporous silica/ chitosan | $Hg^{2+}{}_{(g)}$ | pH, 5.5–6, 298 K | 314.1 | | | 478.5 | [131] |
| | 4-allyloxy benzaldehyde and melamine | | pH 5, 298 K | 335 | 0.54 | – | 312 | [191] |

**Note**; AC represents activated carbon.
$Hg_{(aq)}$ represents aqueous mercury.
$Hg^{2+}{}_{(g)}$ represents gaseous mercury.
ITQ-2 zeolite represents Sodium metasilicate and Sodium meta aluminate infused with Co and Mn.

### 4.2. Modern practices in the adsorption of mercury from wastewater

Several factors are important in the adsorption of Hg from aqueous solutions, including the solution chemistry, such as pH, and properties of the adsorbent, including pore size and distribution. For interactions to be attractive, there must be a harmonious charge opposition between $Hg^{2+}$ and the net surface charge of the adsorbent, creating an attractive force responsible for chemical and physical adsoprtion seen in Fig. 3b. Electrostatic interactions predominantly manifest when the adsorbent bears a net negative surface charge within the pH range of 1–5.59.

Traditional carbonaceous adsorbents include activated carbon [106] and biomass [26], while modernistic ones include graphene and carbon nanotubes (CNT). As seen in Table 4, the adsorption capacities for carbonaceous adsorbents range from 0.2 to 85.6 mg $g^{-1}$, attaining abatements efficiencies >87%, depending on the original carbon matrix and the functional surface groups presence. As evident in Table 4, sulfidation is the primary procedure for functionalizing AC by using S, $SO_2$, and $Na_2S$ to form thiol (-SH) and ($SO_3H$) functional groups. The thiol functional groups from strong covalent bonds with Hg. Hg is predominantly captured as HgS for AC impregnated with sulfur. On the other hand, in unimpregnated AC and AC impregnated with $SO_2$, Hg is eliminated through physisorption, where Hg attaches to the carbon surface through weak van der Waals forces. The adsorption of Hg on AC is stable for permanent sequestration with leachate concentrations far below 0.2 mg $L^{-1}$ [121]. Biochar also has acceptable Hg removal efficiencies whereby it captures Hg from wastewater through physical entrapment. Furthermore, the moisture content in the biomass decomposes under heat to form radicals such as phenolic hydroxyl and carboxylic groups that form complexes with Hg ions through electrostatic interactions and hydrogen bonding. The torrefaction or pyrolysis temperature influences the dominant functional groups and, consequently, the adsorption mechanism, where biochar generated from torrefaction temperatures of 300 °C, 450 °C, and 600 °C has Hg sorption capacities of 24.2 mg $g^{-1}$, 18.8 mg $g^{-1}$, and 15.1 mg $g^{-1}$ based on Langmuir isotherm. For biochar developed at pyrolysis temperatures of 300 °C and 450 °C, phenolic hydroxyl (Ph-OH) and carboxylic (C(=O)OH) functional groups adsorb more Hg than biochar from 600 °C pyrolysis temperature, where Hg adsorbs on graphite-like domains on the aromatic structure [124]. To improve biochar's Hg immobilization efficiency, it is impregnated with calcium polysulfides (CaSx), which precipitates 50% of inorganic Hg [125].

Metal-based adsorbents are popular due to their availability and cost [118]. Their adsorption capacities range from 0.5 to 14.8 mg $g^{-1}$, as summarized in Table 4. CaO and $CaCO_3$, with a mesoporous silica structure, successfully adsorbed $Hg^{2+}$ through ion exchange [126]. On the other hand, their alkaline active sites were inert to $Hg^0$. Adding oxidants such as $KMnO_4$ and $NaClO_2$ improves the adsorption potential of $HgCl_2$ on $Ca(OH)_2$ beyond 85% [127]. As seen in Table 4, Dimercaprol, a chelating agent, selectively targets specific Hg species and is commonly applied to functionalize metal-based adsorbents. Other adsorbents, including $Fe_3O_4$, $Al_2O_3$, MnO, Ag, $V_2O_5$, $Mg(OH)_2$, and zeolites adsorb HG through surface complexation with functional groups. Additional potential mechanisms for eliminating $Hg^{2+}$ in aqueous matrices include electricity neutralization, hydrophobic interactions, and surface adsorption [128]. Metal-based adsorbents are commonly applied due to their stability at high temperatures, high adsorption potential, and reversibility of the adsorption reaction, which facilitates regeneration for repeated applications [118]. They are also compatible with other adsorbents, graphene-modified Mn-based oxide, and magnetic carbon nanotubes ($Fe_3O_4$/CNTs). Electron-rich amino groups donate electrons in chelation, resulting in metal complexation [129]. Other recent methods, including metal-organic framework (MOF) comprising metal ions linked with organic bridging ligands and chelation, have been applied to abstract Hg [115]. A key drawback is the susceptibility to poisoning by $SO_2$, as seen in the investigation involving MnOx-$CeO_2$/y-$Al_2O_3$ catalyst at low temperatures [130].

Polymer composite adsorbents adsorb Hg more rapidly and efficiently than carbonaceous and metal-based adsorbents, as evident in the Qmax values, pore volumes, and BET surface areas presented in Table 4. Their adsorption capacities range from 168.1 to 1216 mg $g^{-1}$, whereby potential mechanisms include pore filling and hydrogen bonding. They have drawn the scientific community's attention due to their high tolerance for functional groups such as amine (-$NH_2$) and hydroxyl (-OH), which have a high affinity for Hg species. The –$NH_2$ and –OH functional groups donate electrons to form coordination complexes with Hg, causing high adsorption capacities. As

**Table 5**
Indicating the adsorption isotherms used for describing Hg adsorption potentials for different matrices.

| Model | Equation | Details | References |
|---|---|---|---|
| Langmuir | $\frac{1}{q_e} = \frac{1}{q_m} + \frac{1}{K_L q_m C_e}$ | It describes monolayer adsorption | [123] |
| Freundlich | $\log q_e = \log K_f + \frac{1}{n}\log C_e$ | It describes multilayer adsorption and heterogeneous adsorption sites | [192] |
| Dubinin-Radushkevich | $\ln q_e = \ln Q_0 - K_{DR}[RT\ln\left(1+\frac{1}{C_e}\right)]^2$<br>$E = \frac{1}{\sqrt{2K_{DR}}}$ | It indicates the type of adsorption process, including physical, chemical, or based on calculated mean adsorption energy on the adsorbent's surface | [123] |
| Note; $q_e$ is the mass of Hg adsorbed per unit mass of adsorbent (mg/g) at equilibrium $q_m$ constant for maximum monomer saturation capacity (mg/g)<br>$K_L$ is the affinity of the adsorbate towards the adsorbent<br>$C_e$ is the equilibrium concentration (mg/L)<br>Freundlich constant ($K_f$) | | R is the universal gas constant (8.314 J/mol.K)<br>T is the temperature (Kelvin)<br>$K_{DR}$ gives the mean adsorption energy (kJ/mol)<br>$E$ is the attraction force between the adsorbate and the adsorbent | |

indicated in Table 4, polymer composite adsorbents are functionalized by grafting them with acrylonitrile and hydroxylamine hydrochloride. Despite their remarkable Hg elimination potentials, they have the drawbacks of low mechanical strength, quickly dissolving in acid media, and difficulties in separation and recovery [131].

The application of adsorbents to capture aqueous Hg is a promising technique. The three categories of adsorbents described herein are adopted in different waste streams depending on their solubility and recovery techniques. Although it is difficult to compare the performance of adsorbents mentioned herein due to disparities in the experimental setups and data presentation, their adsorption capacities rank as polymer-based > carbonaceous > metal-based adsorbents. With regards to selectivity, polymer-based ones have the highest. To re-use saturated adsorbents, regeneration is performed through heating, plasma, ultrasonic, and electrochemical methods. Only carbonaceous adsorbents are thermally stable; therefore, plasma, ultrasonic, and electrochemical methods are more useful for metal-based and polymer-based adsorbents. However, they are cost-intensive and currently unachievable on an industrial scale. Metal-based adsorbents are applicable in high-temperature environments and are also reusable. Overall, further research is required to establish the practicability of their application.

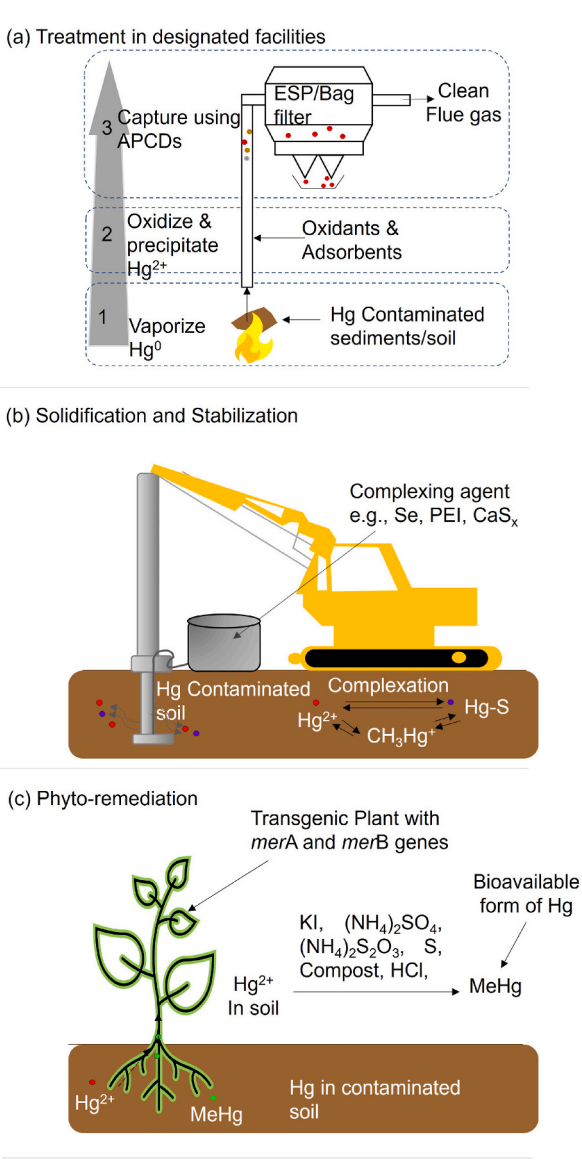


**Fig. 4.** Remediation techniques for Hg-contaminated soil and sediments, including (a) heat treatment, adapted from Refs. [118,195] (b) solidification and immobilization using complexation agents, adapted from Ref. [196] and (c) phytoremediation of biologically available mercury, adapted from [134,197].

### 4.3. Comprehensive approaches for restoring mercury-contaminated soil and sediments

Soil quality criteria (SQC) are applied to assess the concentrations of Hg, where, for instance, in the European Union (EU), the SQC ranges between 1 and 1.5 mg $kg^{-1}$ [30]. The sequential extraction process is applied to assess the risk of Hg to the environment [102]. Remediation approaches are applied for soils exceeding the SQC, including excavation for treatment in designated facilities in Fig. 4a [132], solidification and stabilization using complexation agents in Fig. 4b [133], and phytoremediation [134] in Fig. 4c. The Hg concentrations in soils is likely to exceed the SQC in abandoned gold mines, chlor-alkali, and mono vinyl chloride plants [16].

#### 4.3.1. Integrated strategies: from mercury contamination mapping to remediation

Long-term monitoring and evaluation of matrices commonly associated with exposure to Hg, for instance, air, water, sediments, soil, and foods, helps determine potential mitigation measures [13]. Therefore, for industrial cities with urban rivers and coastal zones, it is crucial to map emission sources upstream and in the vicinity of the coastal zone to gain an improved knowledge of source-receptor relationships, transformations, and Hg biogeochemical cycles. Environmental protection agencies set Hg limits in environmental matrices to prevent contamination and exposure to aquatic and terrestrial life. For instance, the EU has an environmental quality standard of 20 μg $kg^{-1}$ [135]. The USEPA limit for Hg in water is 1.4 μg $kg^{-1}$, while that of the Brazilian Environmental Protection Agency (CONAMA) is 2 μg $kg^{-1}$ [136].

To simulate occupational exposures, the necessary preparations are made to provide baseline corrections before the exposure experiments. Drops of $Hg^0$ or $HgCl_2$ are used in the adsorption chambers, whereby for long-term exposure, the tissues under consideration are kept at 40 °C for about 20 days, maintaining the same heating cycle (8 h $day^{-1}$). Sampled populations are usually divided into groups, where, in addition to collecting hair, toenails, fingernails, and urine and samples, investigations involving human populations require the filling of general lifestyle and health examination questionnaires [6]. Specific important information includes potential occupational exposures, the amount and frequency of consuming rice and fish, known health conditions, and the number of amalgam fillings [54]. Typically, Biological samples, such as muscle, scutes, hair, and nails, undergo ultrasonification for 1 h in 100 mL of a 1% (w/v) RBS 25 detergent to remove surface impurities and achieve standardized background levels. Subsequently, they are rinsed four times with 100 mL of deionized water. After that, they are oven-dried at 50 °C for 24 h and equilibrated at room temperature and ambient humidity for 5 h before further analysis [54].

Approximately 10 mg of the sample is pre-digested in 5 mL of $HNO_3$ for 20 min, followed by autoclave digestion in sealed glass vessels at 100 °C for 90 min. The resulting digests were preserved at 4 °C until subsequent analysis. Before analysis, digested samples are diluted to 5% acid concentration. Sequential mixing with a blank solution (5% $HNO_3$) followed by reaction with a reductant (2% $SnCl_2$) in the sample valve is performed on the diluted digest to generate $Hg^0$ vapor, which, is in turn, purged with argon gas from the gas-liquid separator through the dryer into the atomizer of cold vapor atomic fluorescence spectroscopy for analysis [11].

Bioindicators and isotopes are applied to map Hg concentrations in the environment. For instance, muscles and scutes of sea turtles were applied to monitor long-term Hg exposure in marine environments across New York State, USA, where concentrations ranged between 0.041 and 1.5 μg $g^{-1}$ and 0.47–7.43 μg $g^{-1}$, respectively [137]. In a systemic review, turtles' scute tissues from the South Atlantic Ocean had the highest Hg concentrations, implying the most contamination [67]. Elsewhere, the concentration of total Hg in 86 out of 90 fish muscles exceeded EU food safety regulations [138]. For individual fishes, Hg content was proportional to size and weight, with functional proteins in the muscles, livers, and gonads of three common fish species, including *Merluccius merluccius*, *Mullus surmuletus*, and *Solea solea* having the highest concentrations. Specifically, the average masses of MeHg in the muscles of the three species were 177 ng $g^{-1}$, 235 ng $g^{-1}$, and 87 ng $g^{-1}$; in the liver, they were 73 ng $g^{-1}$, 225 ng $g^{-1}$, and 66 ng $g^{-1}$; in the gonads, they were 41 ng $g^{-1}$, 67 ng $g^{-1}$, and 20 ng $g^{-1}$ respectively. High metabolic activity in the liver for detoxication causes it to accumulate more Hg than other organs [138]. For some apex predators, such as the polar bear, the kidney is a more critical organ for the deposition of Hg than the liver and muscles. The average Hg concentrations in polar bears' kidneys were 12.7 μg $g^{-1}$ pre-2000 and 18 μg $g^{-1}$ post-2000 [139], implying accumulation of Hg in the arctic habitats.

Long-term trends on Hg concentrations in terrestrial environments are performed using *Macrolepiota procera*, a species of wild edible mushrooms shown to accumulate up to 1.98 ± 68.2 mg $kg^{-1}$ of Hg, which exceeds other green plants and cultivated edible mushrooms [140]. Hg concentrations in tubes and pores were 3.86 mg $kg^{-1}$ of dry weight and exceeded that of the flesh cap, which was 1.82 mg $kg^{-1}$ of dry weight [141]. Overall, the concentrations of Hg in wild edible mushrooms depend on the species' element-enrichment ability, environmental pollution, and geochemical properties.

Knowledge of stable mercury isotopes is important to investigate Hg biogeochemical cycles and their deposition in water sediments [67]. The isotopes of $^{202}Hg$ and $^{204}Hg$ and stable isotopes of $^{13}C$, $^{15}N$, and $^{34}S$ indicate an organism's trophic level [85]. Stable nitrogen isotope $^{15}N$ gets 2–4% enrichment in each trophic level, while that of carbon $^{13}C$ gets enriched by 0.5–1% for each incremental trophic level. Therefore, the concentration of MeHg is usually proportional to that of the above mentioned stable isotopes. Furthermore, the abundance of $^{13}C$ is applied to investigate carbon availability for methylation [22]. For investigation involving Hake, red mullet, and Sole, which are carnivores, omnivores, and herbivores, respectively, the former had the highest nitrogen isotopic rations. This was consistent with the relative trophic position of the three fish species [138]. Three isotopes of Hg, including $^{202}Hg$, $^{199}Hg$, and $^{200}Hg$, provide fingerprints of Hg sources in aquatic sediments [142]. They also provide information on the source and contamination pathway. For instance, fresh effluents from industrial plants, wastewater plants, and mining tailing runoffs lack $^{199}Hg$, and $^{200}Hg$, while coastal sediments from historical emissions have $^{199}Hg$, and $^{200}Hg$ [74].

#### 4.3.2. Advanced techniques for mercury remediation

As presented in Fig. 4a, designated facilities for Hg control usually incinerate Hg-containing waste to volatilize the Hg, followed by

capture using appropriate APCDs, mainly activated carbon injection and filtration [106]. This approach is fast and reliable. However, it is unsustainable due to its energy-intensive nature and damage to the soil [132]. A heating temperature of 250 °C adequately volatilizes $Hg^0$ from soils. It also induces some irreversible chemical and physical transformations in these soils.

Solidification and stabilization approaches presented in Fig. 4b use chemical agents to remediate large areas of contaminated soil and sediments. Complexation agents such as humic acid, Polyethylenimine (PEI), and Se reduce the mobility and bioavailability of Hg through interactions via ligand-induced oxidative complexation [143]. Humic acid (HA) fixes Hg in soils with low clay contents and reduces leaching into waterways [21]. Reduced HA and $Hg^0$ had strong complexation interaction in dark and anaerobic condition [144]. Other complexation agents include Sodium sulfide ($Na_2S$), sodium hydrosulfide (NaHS), 2,4,6-trimercaptotriazine trisodium (TMT), and sodium dithiocarbamate (DTCR). Their complexation mechanisms involve $Na^+$ dissociation and Hg–S bond formation, where their efficiencies reach 5–20%, 50–62% of the Hg remains in aqueous state, and 8–30% escapes as GEM [15].

Phytoremediation for Hg-contaminated soils is affected by plant species, soil, meteorological conditions, Hg heterogeneity, and bioavailability [134]. Hg lacks biological function in plants; therefore, this approach has low extraction efficiencies due to the lack of plants with exceptional capacities to accumulate Hg [21]. Consequently, essential considerations in the choice of plants for phytoremediation include translocation factor (TF) and bioaccumulation factor (BAF) [134]. For an investigation involving three plant species, Brassica juncea var.LDZY, Brassica juncea var.ASKYC, and Brassica napus var. ZYYC, the former, had the highest BAF, elsewhere, Axonopus compressus had B*AF* value of >1 [145],. To improve the efficiency of phytoremediation, bacterial genes; *mer*A and *mer*B, which encode mercuric reductase and organomercurial lyase, respectively, are injected in some plants such as arabidopsis, tobacco, and yellow poplar, resulting in transgenic plants with Hg accumulation potential [146]. Since the process is slow, chemical accelerators are added, including humic acid, ammonium sulfate, ammonium thiosulfate, sodium sulfite, sodium thiosulfate, HCl, and sulfur fertilizers [134]. Thiosulfate ($S_2O_3^{2-}$) undergoes chemical association with Hg in contaminated soils, increasing the solubility of THg and improving its susceptibility to phytoextraction. Adding compost from green wastes and nitrilotriacetic acid increased the translocation efficiency of Hg by 128–154% and consequently improved Hg accumulation by *Lepidium sativum* L [147]. The concentration of chemical accelerators added is carefully evaluated to prevent excessive levels of bioavailable Hg from leaching into ground and surface waters.

## 5. Frontier emerging issues in Hg contamination

Recent advances in analytical methods and technologies have enhanced the ability to detect and quantify Hg at ultra-low concentrations. Other techniques, such as remote sensing, provide valuable data for spatial and temporal patterns required for Global Hg monitoring. These techniques contribute to a more detailed understanding of mercury distribution and behavior in various environmental matrices. A contemporary concern has surfaced on the long-term consequences of the interactions between Hg and emerging contaminants such as pharmaceuticals, microplastics, and personal care products in aquatic environments. For instance, recent studies indicate that microplastics and nanoplastics adsorb Hg as vectors and thus potentially influencing its bioavailability and impact to the ecosystem [148]. In high-nutrient aquatic environments, eutrophic conditions enhance methylation to form MeHg, a more toxic and bioavailable form of Hg [149]. This emergent concern underscores the intricate and multifaceted character of emerging contaminants entwined with mercury (Hg) pollution in aquatic environments. It emphasizes the imperative for a nuanced and rigorous investigation into their intricate interplay within aquatic ecosystems.

Climate change will impact the cycling of legacy emissions and overall mercury dynamics by influencing precipitation, temperatures, and perennially frozen subsoils. In turn, this will significantly change the transportation and transformation of Hg in different ecosystems. Warmer temperatures in the Arctic degrade the permafrost, releasing MeHg, which translocates to the Arctic sediments and soils [150]. Since biomass burning contributes to 13% of the total natural Hg emissions, the expected increase in the intensity of wildfires will significantly increase legacy Hg emissions [151].

Strategies advocated by the Minamata Convention involve banning new Hg mines and closing existing ones [46]. Another approach involves phasing out products and industrial processes that require Hg as inputs and adopting Hg-free alternatives that are technically and economically feasible [152]. Specific products to be phased out by this ban include batteries whose Hg content is >2%, Hg vapor lamps, biocides pesticides, topical antiseptics, and cosmetics containing Hg contents.

Adopting alternative Hg-free technologies in gold and other metallurgical processes, cement manufacturing, coal combustion, and vinyl chloride monomer processing will also reduce Hg emissions. For instance, artisanal gold miners could adopt amalgamation of concentrates or cyanidation [26]. Direct chlorination of ethylene [41] and oxychlorination using a catalyst [153] to produce vinyl chloride are alternative methods for vinyl chloride monomer production instead of the traditional acetylene hydrochlorination method with Hg as a catalyst. Using membrane cell electrolysis to make caustic soda and chlorine gas has significantly replaced the traditional Hg cell electrolysis method applied in chlor-alkali plants [54]. Researchers are trying to use gene modification technologies to develop transgenic plants with high Hg bioaccumulation potential for the in-situ remediation of contaminated soils.

## 6. Conclusions

There is high uncertainty in anthropogenic Hg emissions, where the most significant sources include artisanal small-scale gold mining, coal combustion, cement production, and waste combustion. The dominance of combustion sources in Hg emissions suggests the need to improve the currently available strategies for capturing Hg in flue gases. Technological advancements and alternative methods are required to control Hg emissions from ASGM, coal combustion, and cement manufacturing. Techniques for mapping Hg concentrations in environments using human and animal tissues help understand the extent of Hg contamination. Global hotspots for

Hg contamination are concentrated in Asia, South America, and Sub-Saharan Africa due to Hg-intensive ASGM, high dependence on coal for energy, and other socioeconomic factors. These regions should innovatively adopt carbonaceous, metal-, and polymer-based adsorbents to capture Hg from contaminated soils and water. It is difficult to compare the performance of different adsorbents in literature due to disparities in the experimental setup and data presentation. However, polymer-based adsorbents have higher performances due to higher tolerances for $–NH_2$ and –OH functional groups. They have the drawback of regeneration due to their instability. Carbonaceous adsorbents have acceptably high adsorption capacities and are also thermally stable. Metal-based adsorbents have the lowest adsorption capacities of the three categories, but they are compatible with other adsorbents. In addition to the provisions of the Minamata Convention, which advocates the development of Hg-free techniques for industrial applications, efforts on climate change should remain on course to prevent legacy emissions.

## Data availability statement

Data used in this article will be made available on request.

## CRediT authorship contribution statement

**Hsin-Chieh Kung:** Writing – original draft, Funding acquisition, Conceptualization. **Chien-Hsing Wu:** Writing – review & editing, Investigation, Data curation. **Bo-Wun Huang:** Writing – review & editing, Supervision, Funding acquisition. **Guo-Ping Chang-Chien:** Writing – review & editing, Supervision, Funding acquisition, Conceptualization. **Justus Kavita Mutuku:** Writing – review & editing, Writing – original draft, Formal analysis, Conceptualization. **Wan-Ching Lin:** Writing – review & editing, Writing – original draft, Supervision, Conceptualization.

## Declaration of competing interest

The authors declare that they have no known competing financial interests or personal relationships that could have appeared to influence the work reported in this paper.

## References

[1] Z. Rahman, V.P. Singh, The relative impact of toxic heavy metals (THMs)(arsenic (As), cadmium (Cd), chromium (Cr)(VI), mercury (Hg), and lead (Pb)) on the total environment: an overview, Environ. Monit. Assess. 191 (2019) 1–21.
[2] H. Yan, et al., Millennial mercury records derived from ornithogenic sediment on Dongdao Island, South China Sea, Journal of Environmental Sciences 23 (9) (2011) 1415–1423.
[3] R.A. Lavoie, et al., Biomagnification of mercury in aquatic food webs: a worldwide meta-analysis, Environmental science & technology 47 (23) (2013) 13385–13394.
[4] J. Kall, A. Just, M. Aschner, What is the risk? Dental amalgam, mercury exposure, and human health risks throughout the life span, Epigenetics, the environment, and children's health across lifespans (2016) 159–206.
[5] M. Neghab, et al., Health effects associated with long-term occupational exposure of Employees of a chlor-alkali plant to mercury, Int. J. Occup. Saf. Ergon. 18 (1) (2012) 97–106.
[6] A. Castaño, et al., Mercury levels in blood, urine and hair in a nation-wide sample of Spanish adults, Sci. Total Environ. 670 (2019) 262–270.
[7] P.N. Obasi, B.B. Akudinobi, Potential health risk and levels of heavy metals in water resources of lead–zinc mining communities of Abakaliki, southeast Nigeria, Appl. Water Sci. 10 (7) (2020) 1–23.
[8] T.W. Clarkson, L. Magos, The Toxicology of mercury and its chemical compounds, Crit. Rev. Toxicol. 36 (8) (2006) 609–662.
[9] G. Bjørklund, et al., Insights into the potential role of mercury in Alzheimer's disease, J. Mol. Neurosci. 67 (4) (2019) 511–533.
[10] S. Llop, F. Ballester, K. Broberg, Effect of gene-mercury interactions on mercury Toxicokinetics and neurotoxicity, Current Environmental Health Reports 2 (2) (2015) 179–194.
[11] L. Castriotta, et al., The role of mercury, selenium and the Se-Hg antagonism on cognitive neurodevelopment: a 40-month follow-up of the Italian mother-child PHIME cohort, Int. J. Hyg Environ. Health 230 (2020) 113604.
[12] H.K. Galappaththi, I. Suraweera, Risk of Mercury exposure during childhood: a review of Sri Lankan situation, Rev. Environ. Health 35 (3) (2020) 229–232.
[13] H. Angot, et al., Global and local impacts of delayed mercury mitigation efforts, Environmental science & technology 52 (22) (2018) 12968–12977.
[14] O. Ajala, et al., A review of emerging micro-pollutants in hospital wastewater: environmental fate and remediation options, Results in Engineering (2022) 100671.
[15] C.-J. Hsu, et al., Gaseous mercury re-emission from wet flue gas desulfurization wastewater aeration basins: a review, J. Hazard Mater. 420 (2021) 126546.
[16] J. Xu, et al., Sources and remediation techniques for mercury contaminated soil, Environ. Int. 74 (2015) 42–53.
[17] E.G. Pacyna, et al., Global emission of mercury to the atmosphere from anthropogenic sources in 2005 and projections to 2020, Atmospheric environment 44 (20) (2010) 2487–2499.
[18] F. Steenhuisen, S. Wilson, Development and application of an updated geospatial distribution model for gridding 2015 global mercury emissions, Atmospheric environment 211 (2019) 138–150.
[19] L. Yang, et al., Toxicity of mercury: Molecular evidence, Chemosphere 245 (2020) 125586.
[20] A.D. Singh, et al., Critical review on biogeochemical dynamics of mercury (Hg) and its abatement strategies, Chemosphere (2023) 137917.
[21] B. Gworek, W. Dmuchowski, A.H. Baczewska-Dąbrowska, Mercury in the terrestrial environment: a review, Environ. Sci. Eur. 32 (1) (2020) 128.
[22] H. Elsayed, et al., Methylmercury bioaccumulation among different food chain levels in the EEZ of Qatar (Arabian Gulf), Regional Studies in Marine Science 37 (2020) 101334.
[23] G.-C. Fang, Y.-S. Wu, T.-H. Chang, Comparison of atmospheric mercury (Hg) among Korea, Japan, China and Taiwan during 2000–2008, J. Hazard Mater. 162 (2–3) (2009) 607–615.
[24] X. Jiang, F. Wang, Mercury emissions in China: a general review, Waste Disposal & Sustainable Energy 1 (2) (2019) 127–132.
[25] S. Liang, et al., Socioeconomic drivers of mercury emissions in China from 1992 to 2007, Environmental science & technology 47 (7) (2013) 3234–3240.
[26] A. Yoshimura, K. Suemasu, M.M. Veiga, Estimation of mercury Losses and gold production by artisanal and small-scale gold mining (ASGM), Journal of Sustainable Metallurgy 7 (3) (2021) 1045–1059.
[27] A. Joy, A. Qureshi, Reducing mercury emissions from coal-fired power plants in India: possibilities and challenges, Ambio 52 (1) (2023) 242–252.

[28] J. Huang, et al., Atmospheric mercury pollution at an urban site in central Taiwan: mercury emission sources at ground level, Chemosphere 87 (5) (2012) 579–585.
[29] K. Kogut, J. Górecki, P. Burmistrz, Opportunities for reducing mercury emissions in the cement industry, J. Clean. Prod. 293 (2021) 126053.
[30] O. Gyamfi, et al., Contamination, exposure and risk assessment of mercury in the soils of an artisanal gold mining community in Ghana, Chemosphere 267 (2021) 128910.
[31] U.G.M. Assessment, UN Environment, Chemicals and Health Branch, Geneva, Switzerland, 2019.
[32] D.G. Streets, et al., Global and Regional Trends in Mercury Emissions and Concentrations, 2010–2015, vol. 201, Atmospheric Environment, 2019, pp. 417–427.
[33] S. Keane, et al., Mercury and artisanal and small-scale gold mining: review of global use estimates and considerations for promoting mercury-free alternatives, Ambio 52 (5) (2023) 833–852.
[34] Y. Cheng, et al., Examining the inconsistency of mercury flow in post-Minamata Convention global trade concerning artisanal and small-scale gold mining activity, Resour. Conserv. Recycl. 185 (2022) 106461.
[35] X. Wang, L. Yan, Driving factors and decoupling analysis of fossil fuel related-carbon dioxide emissions in China, Fuel 314 (2022) 122869.
[36] S. Zhao, et al., A review on mercury in coal combustion process: content and occurrence forms in coal, transformation, sampling methods, emission and control technologies, Prog. Energy Combust. Sci. 73 (2019) 26–64.
[37] S. Wang, et al., A review of atmospheric mercury emissions, pollution and control in China, Front. Environ. Sci. Eng. 8 (2014) 631–649.
[38] S. Alam, et al., Selection of waste to energy technologies for municipal solid waste management—towards achieving sustainable development goals, Sustainability 14 (19) (2022) 11913.
[39] N. Pirrone, et al., Global mercury emissions to the atmosphere from anthropogenic and natural sources, Atmos. Chem. Phys. 10 (13) (2010) 5951–5964.
[40] W.-T. Tsai, Multimedia pollution prevention of mercury-containing waste and articles: case study in Taiwan, Sustainability 14 (3) (2022) 1557.
[41] K. Zhou, et al., Continuous vinyl chloride monomer production by acetylene hydrochlorination on Hg-free bismuth catalyst: from lab-scale catalyst characterization, catalytic evaluation to a pilot-scale trial by circulating regeneration in coupled fluidized beds, Fuel Process. Technol. 108 (2013) 12–18.
[42] G. Martinez, et al., Mercury contamination in riverine sediments and fish associated with artisanal and small-scale gold mining in Madre de Dios, Peru, Int. J. Environ. Res. Publ. Health 15 (8) (2018) 1584.
[43] R. Soni, et al., A systematic review on mercury toxicity from dental amalgam fillings and its management strategies, Journal of scientific research 2012 (56) (2012) 81–92.
[44] D. Lobner, M. Asrari, Neurotoxicity of dental amalgam is mediated by zinc, Journal of dental research 82 (3) (2003) 243–246.
[45] N.A. Khan, et al., Occurrence, sources and conventional treatment techniques for various antibiotics present in hospital wastewaters: a critical review, TrAC, Trends Anal. Chem. 129 (2020) 115921.
[46] D.C. Evers, et al., Evaluating the effectiveness of the Minamata convention on mercury: principles and recommendations for next steps, Sci. Total Environ. 569 (2016) 888–903.
[47] L. Rani, A.L. Srivastav, J. Kaushal, Bioremediation: an effective approach of mercury removal from the aqueous solutions, Chemosphere 280 (2021) 130654.
[48] A. Chalkidis, et al., Mercury in natural gas streams: a review of materials and processes for abatement and remediation, J. Hazard Mater. 382 (2020) 121036.
[49] F. Kho, et al., Current understanding of the ecological risk of mercury from subsea oil and gas infrastructure to marine ecosystems, J. Hazard Mater. (2022) 129348.
[50] H. Zheng, et al., Combination of sequential cloud point extraction and hydride generation atomic fluorescence spectrometry for preconcentration and determination of inorganic and methyl mercury in water samples, Microchem. J. 145 (2019) 806–812.
[51] U.S. Nair, et al., Diurnal and seasonal variation of mercury species at coastal-suburban, urban, and rural sites in the southeastern United States, Atmos. Environ. 47 (2012) 499–508.
[52] A.L. Gagliano, et al., Degassing and cycling of mercury at Nisyros volcano (Greece), Geofluids 2019 (2019) 4783514.
[53] G.-R. Sheu, et al., Temporal distribution and potential sources of atmospheric mercury measured at a high-elevation background station in Taiwan, Atmos. Environ. 44 (20) (2010) 2393–2400.
[54] A.A.S. Elgazali, et al., Reactive gaseous mercury is generated from chloralkali factories resulting in extreme concentrations of mercury in hair of workers, Sci. Rep. 8 (1) (2018) 3675.
[55] C.S. Eckley, et al., Soil–air mercury flux near a large industrial emission source before and after closure (Flin Flon, Manitoba, Canada), Environmental Science & Technology 49 (16) (2015) 9750–9757.
[56] J.Y. Lu, W.H. Schroeder, Annual time-series of total filterable atmospheric mercury concentrations in the Arctic, Tellus B 56 (3) (2004) 213–222.
[57] X. Fu, et al., Atmospheric gaseous elemental mercury (GEM) concentrations and mercury depositions at a high-altitude mountain peak in south China, Atmos. Chem. Phys. 10 (5) (2010) 2425–2437.
[58] Z. Wang, et al., Mercury fluxes and pools in three subtropical forested catchments, southwest China, Environmental Pollution 157 (3) (2009) 801–808.
[59] M. Méndez-López, et al., The role of afforestation species as a driver of Hg accumulation in organic horizons of forest soils from a Mediterranean mountain area in SW Europe, Sci. Total Environ. 827 (2022) 154345.
[60] J. Zhou, et al., Vegetation uptake of mercury and impacts on global cycling, Nat. Rev. Earth Environ. 2 (4) (2021) 269–284.
[61] E.K. Miller, et al., Estimation and mapping of wet and dry mercury deposition across northeastern North America, Ecotoxicology 14 (2005) 53–70.
[62] M.R. Risch, et al., Litterfall mercury dry deposition in the eastern USA, Environmental Pollution 161 (2012) 284–290.
[63] M. Ma, et al., Gaseous mercury emissions from subtropical forested and open field soils in a national nature reserve, southwest China, Atmos. Environ. 64 (2013) 116–123.
[64] A. During, et al., Mercury volatilization from three floodplain soils at the Central Elbe River, Germany, Soil Sediment Contam. 18 (4) (2009) 429–444.
[65] C.W. Moore, M.S. Castro, Investigation of factors affecting gaseous mercury concentrations in soils, Sci. Total Environ. 419 (2012) 136–143.
[66] B.K.K.K. Jinadasa, S.W. Fowler, Critical review of mercury contamination in Sri Lankan fish and aquatic products, Mar. Pollut. Bull. 149 (2019) 110526.
[67] M.M. Al-Sulaiti, L. Soubra, M.A. Al-Ghouti, The causes and effects of mercury and methylmercury contamination in the marine environment: a review, Current Pollution Reports 8 (3) (2022) 249–272.
[68] E. Suess, et al., Mercury loads and fluxes from wastewater: a nationwide survey in Switzerland, Water Res. 175 (2020) 115708.
[69] A. Gallorini, J.-L. Loizeau, Mercury methylation in oxic aquatic macro-environments: a review, J. Limnol. 80 (2) (2021).
[70] K. Wang, G. Liu, Y. Cai, Possible pathways for mercury methylation in oxic marine waters, Crit. Rev. Environ. Sci. Technol. 52 (22) (2022) 3997–4015.
[71] V. Perrot, et al., Identical Hg isotope mass dependent fractionation signature during methylation by sulfate-reducing bacteria in sulfate and sulfate-free environment, Environmental science & technology 49 (3) (2015) 1365–1373.
[72] J. Wang, et al., Role of sulfur biogeochemical cycle in mercury methylation in estuarine sediments: a review, J. Hazard Mater. 423 (2022) 126964.
[73] L. Mao, et al., Mercury contamination in the water and sediments of a typical inland river-lake basin in China: occurrence, sources, migration and risk assessment, J. Hazard Mater. (2023) 130724.
[74] M. Meng, et al., An integrated model for input and migration of mercury in Chinese coastal sediments, Environmental Science & Technology 53 (5) (2019) 2460–2471.
[75] N.V. Smith-Downey, E.M. Sunderland, D.J. Jacob, Anthropogenic impacts on global storage and emissions of mercury from terrestrial soils: insights from a new global model, J. Geophys. Res.: Biogeosciences 115 (G3) (2010).
[76] Y. Wang, et al., Total mercury and methylmercury in rice: exposure and health implications in Bangladesh, Environmental Pollution 265 (2020) 114991.
[77] Y.-S. Hong, Y.-M. Kim, K.-E. Lee, Methylmercury exposure and health effects, J Prev Med Public Health 45 (6) (2012) 353–363.
[78] P. de Almeida Rodrigues, et al., Mercury in aquatic fauna contamination: a systematic review on its dynamics and potential health risks, Journal of Environmental Sciences 84 (2019) 205–218.
[79] B.K.K.K. Jinadasa, et al., Mitigating the impact of mercury contaminants in fish and other seafood—a review, Mar. Pollut. Bull. 171 (2021) 112710.
[80] S.C. Jewett, L.K. Duffy, Mercury in fishes of Alaska, with emphasis on subsistence species, Sci. Total Environ. 387 (1) (2007) 3–27.

[81] E. European Commission, *Commission Regulation (EU) No 165/*2010 of 26 February 2010 Amending Regulation (EC) No 1881/2006 Setting Maximum Levels for Certain Contaminants in Foodstuffs as Regards Aflatoxins, vol. 50, Off. J. Eur. Union, 2010, pp. 8–12.
[82] FSANZ, Australia New Zealand food standards code, Secondary Australia New Zealand food standards code (2007).
[83] H. Canada, Human Health Risk Assessment of Mercury in Fish and Health Benefits of Fish Consumption, Bureau of Chemical Safety, Minister of Health, 2007.
[84] L. Santos-Sacramento, et al., Human neurotoxicity of mercury in the Amazon: a scoping review with insights and critical considerations, Ecotoxicol. Environ. Saf. 208 (2021) 111686.
[85] P. Annasawmy, et al., Mercury concentrations and stable isotope ratios (δ13C and δ15N) in pelagic nekton assemblages of the south-western Indian Ocean, Mar. Pollut. Bull. 174 (2022) 113151.
[86] J. Liu, et al., Mercury pollution in fish from South China Sea: levels, species-specific accumulation, and possible sources, Environ. Res. 131 (2014) 160–164.
[87] D. Kasper, et al., Evidence of elevated mercury levels in carnivorous and omnivorous fishes downstream from an Amazon reservoir, Hydrobiologia 694 (1) (2012) 87–98.
[88] B.K. Jinadasa, E.M. Edirisinghe, I. Wickramasinghe, Total mercury content, weight and length relationship in swordfish (Xiphias gladius) in Sri Lanka, Food Addit. Contam. Part B Surveill 6 (4) (2013) 244–248.
[89] I. Sarvan, et al., Exposure assessment of methylmercury in samples of the BfR MEAL Study, Food Chem. Toxicol. 149 (2021) 112005.
[90] L.-C. Chien, et al., Estimation of acceptable mercury intake from fish in Taiwan, Chemosphere 67 (1) (2007) 29–35.
[91] A.M. Shipp, et al., Determination of a site-specific reference dose for methylmercury for fish-eating populations, Toxicol. Ind. Health 16 (9–10) (2000) 335–438.
[92] R. Pamphlett, et al., Concentrations of toxic metals and essential trace elements vary among individual neurons in the human locus ceruleus, PLoS One 15 (5) (2020) e0233300.
[93] C.C. Bridges, et al., New insights into the metabolism of organomercury compounds: mercury-containing cysteine S-conjugates are substrates of human glutamine transaminase K and potent inactivators of cystathionine γ-lyase, Arch. Biochem. Biophys. 517 (1) (2012) 20–29.
[94] K. Engström, et al., Polymorphisms in ATP-binding cassette transporters associated with maternal methylmercury disposition and infant neurodevelopment in mother-infant pairs in the Seychelles Child Development Study, Environ. Int. 94 (2016) 224–229.
[95] L. Feng, et al., Impact of low-level mercury exposure on intelligence quotient in children via rice consumption, Ecotoxicol. Environ. Saf. 202 (2020) 110870.
[96] P.B. Tchounwou, et al., Review: environmental exposure to mercury and its toxicopathologic implications for public health, Environ. Toxicol. 18 (3) (2003) 149–175.
[97] S.V.K. Naidoo, et al., Oral exposure to cadmium and mercury alone and in combination causes damage to the lung tissue of Sprague-Dawley rats, Environ. Toxicol. Pharmacol. 69 (2019) 86–94.
[98] J. Ni, et al., Relationship between exposure to cadmium, lead, and mercury and the occurrence of urinary incontinence in women, Environ. Sci. Pollut. Control Ser. 29 (45) (2022) 68410–68421.
[99] P. Li, et al., Mercury pollution in Asia: a review of the contaminated sites, J. Hazard Mater. 168 (2–3) (2009) 591–601.
[100] R. Kessler, The Minamata Convention on Mercury: a First Step toward Protecting Future Generations, National Institute of Environmental Health Sciences, 2013.
[101] C.S.C. Wong, et al., Sources and trends of environmental mercury emissions in Asia, Sci. Total Environ. 368 (2) (2006) 649–662.
[102] R. Fernández-Martínez, I. Rucandio, Assessment of a sequential extraction method to evaluate mercury mobility and geochemistry in solid environmental samples, Ecotoxicol. Environ. Saf. 97 (2013) 196–203.
[103] J.-H. Kim, et al., Anthropogenic mercury emission inventory with emission factors and total emission in Korea, Atmos. Environ. 44 (23) (2010) 2714–2721.
[104] L. Wang, et al., Recent advance for NOx removal with carbonaceous material for low-temperature NH3-SCR reaction, Catal. Today 418 (2023) 114053.
[105] L. Cui, et al., Integrated assessment of the environmental and economic effects of an ultra-clean flue gas treatment process in coal-fired power plant, J. Clean. Prod. 199 (2018) 359–368.
[106] F. Takahashi, A. Kida, T. Shimaoka, Statistical estimate of mercury removal efficiencies for air pollution control devices of municipal solid waste incinerators, Sci. Total Environ. 408 (22) (2010) 5472–5477.
[107] Q. Zhou, et al., Elemental mercury capture from flue gas by magnetic recyclable Fe6Mn1-xCexOy sorbent. Part 1. Performance evaluation and regeneration, Fuel 304 (2021) 120723.
[108] J. Yang, J. Guo, J. He, Easy, fast, selective, and simultaneous separation of Hg (II) and oil via loofah-sponge-inspired hierarchically porous membranes, ACS Appl. Mater. Interfaces 14 (23) (2022) 27063–27073.
[109] Q. Wu, et al., New insight into atmospheric mercury emissions from zinc smelters using mass flow analysis, Environmental Science & Technology 49 (6) (2015) 3532–3539.
[110] J.R. Oliveira, et al., Synthesis and characterization of adsorbent materials for the retention of elemental mercury from contaminated tropical soils, Int. J. Environ. Sci. Technol. (2022).
[111] A. Gupta, et al., A review on polyacrylonitrile as an effective and economic constituent of adsorbents for wastewater treatment, Molecules 27 (24) (2022) 8689.
[112] Y. Luo, et al., Efficient municipal wastewater treatment by oxidation ditch process at low temperature: bacterial community structure in activated sludge, Sci. Total Environ. 703 (2020) 135031.
[113] P.N. Bhandari, et al., Oxygen nanobubbles revert hypoxia by methylation programming, Sci. Rep. 7 (1) (2017) 1–14.
[114] E. Suess, et al., Mercury loads and fluxes from wastewater: a nationwide survey in Switzerland, Water Res. 175 (2020) 115708.
[115] T. Velempini, K. Pillay, Sulphur functionalized materials for Hg(II) adsorption: a review, J. Environ. Chem. Eng. 7 (5) (2019) 103350.
[116] T. Phengsaart, et al., Conventional and recent advances in gravity separation technologies for coal cleaning: a systematic and critical review, Heliyon 9 (2) (2023) e13083.
[117] A. Kolker, C.L. Senior, J.C. Quick, Mercury in coal and the impact of coal quality on mercury emissions from combustion systems, Appl. Geochem. 21 (11) (2006) 1821–1836.
[118] Z. Ji, et al., Recent progress on the clean and sustainable technologies for removing mercury from typical industrial flue gases: a review, Process Saf. Environ. Protect. 150 (2021) 578–593.
[119] Y. Hu, H. Cheng, Control of mercury emissions from stationary coal combustion sources in China: current status and recommendations, Environmental Pollution 218 (2016) 1209–1221.
[120] M. Pavlin, et al., Mercury fractionation in gypsum using temperature desorption and mass spectrometric detection, Mass spectrometric approach to mercury fractionation in FGD gypsum 16 (1) (2018) 544–555.
[121] J.W. Graydon, et al., Sorption and stability of mercury on activated carbon for emission control, J. Hazard Mater. 168 (2) (2009) 978–982.
[122] Y. Ma, et al., Graphene enhanced Mn-Ce binary metal oxides for catalytic oxidation and adsorption of elemental mercury from coal-fired flue gas, Chem. Eng. J. 358 (2019) 1499–1506.
[123] A.R. Gupta, et al., One-pot facile approach to design an efficient macro-porous polymeric matrix to remediate Hg(II)and Pb(II) from aqueous medium and its performance evaluation study by mathematical modelling, Environmental Pollution 323 (2023) 121255.
[124] X. Dong, et al., Mechanistic investigation of mercury sorption by Brazilian pepper biochars of different pyrolytic temperatures based on X-ray photoelectron spectroscopy and flow calorimetry, Environmental Science & Technology 47 (21) (2013) 12156–12164.
[125] S.M. Dahlawi, S. Siddiqui, Calcium polysulphide, its applications and emerging risk of environmental pollution—a review article, Environ. Sci. Pollut. Control Ser. 24 (1) (2017) 92–102.
[126] C. Li, et al., Synthetic calcium-based adsorbents for gaseous mercury(II) adsorption from flue gas and study on their mercury adsorption mechanism, Fuel 234 (2018) 384–391.
[127] H. Wang, et al., A critical review on the method of simultaneous removal of multi-air-pollutant in flue gas, Chem. Eng. J. 378 (2019) 122155.

[128] Z.V.P. Murthy, P.A. Parikh, N.B. Patel, Application of β-zeolite, zeolite Y, and mordenite as adsorbents to remove mercury from aqueous solutions, J. Dispersion Sci. Technol. 34 (6) (2013) 747–755.
[129] P.S. Bakshi, et al., Chitosan as an environment friendly biomaterial – a review on recent modifications and applications, Int. J. Biol. Macromol. 150 (2020) 1072–1083.
[130] P. Wang, et al., Catalytic oxidation of Hg0 by MnOx–CeO2/γ-Al2O3 catalyst at low temperatures, Chemosphere 101 (2014) 49–54.
[131] H. He, et al., Thiol-ene click chemistry synthesis of a novel magnetic mesoporous silica/chitosan composite for selective Hg(II) capture and high catalytic activity of spent Hg(II) adsorbent, Chem. Eng. J. 405 (2021) 126743.
[132] D. Ding, et al., A review on the sustainability of thermal treatment for contaminated soils, Environmental Pollution 253 (2019) 449–463.
[133] Z. Gu, et al., Solidification/stabilization of mercury contaminated soil by geopolymer/MoS2 composites, J. Environ. Chem. Eng. 11 (2) (2023) 109546.
[134] Z. Liu, et al., A review on phytoremediation of mercury contaminated soils, J. Hazard Mater. 400 (2020) 123138.
[135] M.D. Jürgens, et al., The presence of EU priority substances mercury, hexachlorobenzene, hexachlorobutadiene and PBDEs in wild fish from four English rivers, Sci. Total Environ. 461–462 (2013) 441–452.
[136] W.D. Constantino, et al., Mercury levels in an environmentally protected estuarine area in Northeast Brazil: partitioning in the water column and transport to the ocean, Environ. Sci. Pollut. Control Ser. 30 (11) (2023) 31383–31394.
[137] M.A. Turnquist, et al., Mercury concentrations in snapping turtles (Chelydra serpentina) correlate with environmental and landscape characteristics, Ecotoxicology 20 (7) (2011) 1599–1608.
[138] T. Mille, et al., Distribution of mercury species in different tissues and trophic levels of commonly consumed fish species from the south Bay of Biscay (France), Mar. Pollut. Bull. 166 (2021) 112172.
[139] M. Dominique, et al., Comparative review of the distribution and burden of contaminants in the body of polar bears, Environ. Sci. Pollut. Control Ser. 27 (26) (2020) 32456–32466.
[140] S. Liu, et al., Research progress on elements of wild edible mushrooms, Journal of Fungi 8 (9) (2022) 964.
[141] J. Árvay, et al., Mercury in scarletina bolete mushroom (Neoboletus luridiformis): intake, spatial distribution in the fruiting body, accumulation ability and health risk assessment, Ecotoxicol. Environ. Saf. 232 (2022) 113235.
[142] L. Schneider, et al., Mercury atmospheric emission, deposition and isotopic fingerprinting from major coal-fired power plants in Australia: insights from palaeo-environmental analysis from sediment cores, Environmental Pollution 287 (2021) 117596.
[143] J. Barron-Zambrano, et al., Mercury removal from aqueous solutions by complexation—ultrafiltration, Desalination 144 (1) (2002) 201–206.
[144] B. Gu, et al., Mercury reduction and complexation by natural organic matter in anoxic environments, Proc. Natl. Acad. Sci. USA 108 (4) (2011) 1479–1483.
[145] I. Chamba, et al., Erato polymnioides–A novel Hg hyperaccumulator plant in ecuadorian rainforest acid soils with potential of microbe-associated phytoremediation, Chemosphere 188 (2017) 633–641.
[146] Y. Sasaki, et al., Generation of mercury-hyperaccumulating plants through transgenic expression of the bacterial mercury membrane transport protein MerC, Transgenic Res. 15 (5) (2006) 615–625.
[147] B. Smolińska, The influence of compost and nitrilotriacetic acid on mercury phytoextraction by Lepidium sativum L, Journal of Chemical Technology & Biotechnology 95 (4) (2020) 950–958.
[148] Z. Gao, et al., Adsorption/desorption of mercury (II) by artificially weathered microplastics: kinetics, isotherms, and influencing factors, Environmental Pollution 337 (2023) 122621.
[149] N. Kozak, et al., Environmental and biological factors are joint drivers of mercury biomagnification in subarctic lake food webs along a climate and productivity gradient, Sci. Total Environ. 779 (2021) 146261.
[150] J. Chételat, et al., Climate change and mercury in the Arctic: abiotic interactions, Sci. Total Environ. 824 (2022) 153715.
[151] A. Francisco López, E.G. Heckenauer Barrón, P.M. Bello Bugallo, Contribution to understanding the influence of fires on the mercury cycle: systematic review, dynamic modelling and application to sustainable hypothetical scenarios, Environ. Monit. Assess. 194 (10) (2022) 707.
[152] H. Selin, et al., Linking science and policy to support the implementation of the Minamata Convention on Mercury, Ambio 47 (2018) 198–215.
[153] H. Ma, et al., Nitrogen-doped carbon-assisted one-pot tandem reaction for vinyl chloride production via ethylene oxychlorination, Angew. Chem. Int. Ed. 59 (49) (2020) 22080–22085.
[154] Q. Wang, et al., Mercury in desulfurization gypsum and its dependence on coal properties in coal-fired power plants, Fuel 293 (2021) 120413.
[155] T. Dziok, et al., Possibility of using alternative fuels in Polish power plants in the context of mercury emissions, Waste Management 126 (2021) 578–584.
[156] Z. Tao, S. Dai, X. Chai, Mercury emission to the atmosphere from municipal solid waste landfills: a brief review, Atmos. Environ. 170 (2017) 303–311.
[157] S. Wang, et al., Characteristics of mercury exchange flux between soil and air in the heavily air-polluted area, eastern Guizhou, China, Atmos. Environ. 41 (27) (2007) 5584–5594.
[158] S. Wang, et al., Mercury concentrations and air/soil fluxes in Wuchuan mercury mining district, Guizhou province, China, Atmos. Environ. 41 (28) (2007) 5984–5993.
[159] S. Wang, et al., Mercury emission to atmosphere from Lanmuchang Hg–Tl mining area, southwestern Guizhou, China, Atmos. Environ. 39 (39) (2005) 7459–7473.
[160] I. Wängberg, et al., Emissions, dispersion and human exposure of mercury from a Swedish chlor-alkali plant, Atmos. Environ. 39 (39) (2005) 7451–7458.
[161] T.-H. Kuo, et al., Atmospheric gaseous mercury in northern Taiwan, Science of the total environment 368 (1) (2006) 10–18.
[162] X. Chen, et al., Mercury in urban soils with various types of land use in Beijing, China, Environmental Pollution 158 (1) (2010) 48–54.
[163] T.F. Frescholtz, M. Sexauer Gustin, Soil and foliar mercury emission as a function of soil concentration, Water Air Soil Pollut. 155 (1) (2004) 223–237.
[164] Y. Yao, et al., Concentrations and speciation of mercury in soil affected by bird droppings, Pol. J. Environ. Stud. 28 (3) (2019) 1451–1459.
[165] D. Peng, et al., Mercury accumulation potential of aquatic plant species in West Dongting Lake, China, Environmental Pollution 324 (2023) 121313.
[166] Q. Li, et al., Total mercury and methylmercury in the soil and vegetation of a riparian zone along a mercury-impacted reservoir, Sci. Total Environ. 738 (2020) 139794.
[167] S. Rahmanpour, N.F. Ghorghani, S.M. Lotfi Ashtiyani, Heavy metal in water and aquatic organisms from different intertidal ecosystems, Persian Gulf, Environ. Monit. Assess. 186 (2014) 5401–5409.
[168] C. Shi, et al., The distribution and risk of mercury in Shenzhen mangroves, representative urban mangroves affected by human activities in China, Mar. Pollut. Bull. 151 (2020) 110866.
[169] P. Calle, et al., Mercury assessment, macrobenthos diversity and environmental quality conditions in the Salado Estuary (Gulf of Guayaquil, Ecuador) impacted by anthropogenic influences, Mar. Pollut. Bull. 136 (2018) 365–373.
[170] G. Cugler de Pontes, et al., Spatial distribution of total mercury and methylmercury in the sediment of a tropical coastal environment subjected to heavy urban inputs, Chemosphere 312 (2023) 137067.
[171] S.C.T. Nicklisch, et al., Mercury levels of yellowfin tuna (Thunnus albacares) are associated with capture location, Environ Pollut 229 (2017) 87–93.
[172] P. Li, et al., Mercury in the seafood and human exposure in coastal area of Guangdong province, South China, Environ. Toxicol. Chem. 32 (3) (2013) 541–547.
[173] M.C. Gabriel, et al., Spatial variability of mercury emissions from soils in a southeastern US urban environment, Environmental Geology 48 (7) (2005) 955–964.
[174] L.P. Wright, L. Zhang, F.J. Marsik, Overview of mercury dry deposition, litterfall, and throughfall studies, Atmos. Chem. Phys. 16 (21) (2016) 13399–13416.
[175] J. Sommar, et al., Seasonal variations in metallic mercury (Hg 0) vapor exchange over biannual wheat–corn rotation cropland in the North China Plain, Biogeosciences 13 (7) (2016) 2029–2049.
[176] A. Carpi, et al., Gaseous mercury emissions from soil following forest loss and land use changes: field experiments in the United States and Brazil, Atmos. Environ. 96 (2014) 423–429.
[177] H. Tan, et al., Atmospheric mercury deposition in Guizhou, China, Sci. Total Environ. 259 (1–3) (2000) 223–230.

[178] A.D. Converse, A.L. Riscassi, T.M. Scanlon, Seasonal variability in gaseous mercury fluxes measured in a high-elevation meadow, Atmos. Environ. 44 (18) (2010) 2176–2185.
[179] C.A. Cooke, et al., Pre-Colombian mercury pollution associated with the smelting of argentiferous ores in the Bolivian Andes, Ambio 40 (1) (2011) 18–25.
[180] O.D. Caicedo Salcedo, et al., Study of mercury [Hg(II)] adsorption from aqueous solution on functionalized activated carbon, ACS Omega 6 (18) (2021) 11849–11856.
[181] L. Tran, et al., Comparative study of Hg(II) adsorption by thiol- and hydroxyl-containing bifunctional montmorillonite and vermiculite, Appl. Surf. Sci. 356 (2015) 91–101.
[182] T. Liu, et al., Review on adsorbents in elemental mercury removal in coal combustion flue gas, smelting flue gas and natural gas, Chem. Eng. J. 454 (2023) 140095.
[183] H. Li, et al., Capture of elemental mercury from flue gas over a magnetic and sulfur-resistant sorbent prepared from Fe-containing sewage sludge activated with sulfuric acid, Fuel 300 (2021) 120938.
[184] H. Ishimori, et al., Establishing soil adsorption testing methods for gaseous mercury and evaluating the distribution coefficients of silica sand, decomposed granite soil, mordenite, and calcium bentonite, Soils Found. 60 (2) (2020) 496–504.
[185] G. Xin, P. Zhao, C. Zheng, Theoretical study of different speciation of mercury adsorption on CaO (001) surface, Proc. Combust. Inst. 32 (2) (2009) 2693–2699.
[186] Y. Ma, et al., Excellent adsorption performance and capacity of modified layered ITQ-2 zeolites for elemental mercury removal and recycling from flue gas, J. Hazard Mater. 423 (2022) 127118.
[187] M. Yavuz, et al., An economic removal of Cu2+ and Cr3+ on the new adsorbents: Pumice and polyacrylonitrile/pumice composite, Chem. Eng. J. 137 (3) (2008) 453–461.
[188] M. Ajmal, et al., Amidoximated poly(acrylonitrile) particles for environmental applications: removal of heavy metal ions, dyes, and herbicides from water with different sources, J. Appl. Polym. Sci. 133 (7) (2016).
[189] Y. Sang, et al., N-rich porous organic polymers based on Schiff base reaction for CO2 capture and mercury(II) adsorption, J. Colloid Interface Sci. 587 (2021) 121–130.
[190] B. Aguila, et al., Efficient mercury capture using functionalized porous organic polymer, Adv. Mater. 29 (31) (2017) 1700665.
[191] J. Ryu, et al., Highly selective removal of Hg(II) ions from aqueous solution using thiol-modified porous polyaminal-networked polymer, Separation and Purification Technology 250 (2020) 117120.
[192] Z. Ali, et al., Complexation of Hg(II) ions with a functionalized adsorbent: a thermodynamic and kinetic approach, Prog. Nucl. Energy 105 (2018) 146–152.
[193] C.T. Driscoll, et al., Mercury as a global pollutant: sources, pathways, and effects, Environmental science & technology 47 (10) (2013) 4967–4983.
[194] N.A.A. Qasem, R.H. Mohammed, D.U. Lawal, Removal of heavy metal ions from wastewater: a comprehensive and critical review, npj Clean Water 4 (1) (2021) 36.
[195] Y. Li, et al., A review on removal of mercury from flue gas utilizing existing air pollutant control devices (APCDs), J. Hazard Mater. 427 (2022) 128132.
[196] C.-Y. Yin, et al., Contaminated Land Remediation Technologies: Current Usage and Applicability in Malaysia, 2006.
[197] E.D. Tiodar, C.L. Văcar, D. Podar, Phytoremediation and microorganisms-assisted phytoremediation of mercury-contaminated soils: challenges and perspectives, Int. J. Environ. Res. Publ. Health 18 (5) (2021) 2435.